EXPLORING TERAHERTZ PULSE ENHANCEMENT THROUGH GOLD NANOPARTICLE DEPOSITION

By

CHRISTOPHER DALL YOUNG

Bachelor of Science in Electrical and Computer Engineering

Brigham Young University

Provo, Utah

2006

Submitted to the Faculty of the
Graduate College of the
Oklahoma State University
in partial fulfillment of
the requirements for
the Degree of
MASTER OF SCIENCE
May, 2009

EXPLORING TERAHERTZ PULSE ENHANCEMENT

THROUGH GOLD NANOPARTICLE DEPOSITION

Thesis Approved:

Dr. Alan Cheville

Thesis Adviser

Dr. Daniel Grischkowsky

Dr. James C. West

Dr. A. Gordon Emslie

Dean of the Graduate College

ACKNOWLEDGMENTS

This project, in many ways, feels like a team effort. I have been the recipient of countless acts of kindness and help while working here at OSU. I wish I had space to thank everyone.

But there are a few who were instrumental to the completion of this project and who offered more assistance then asked of them. These people I would like to acknowledge.

I would like to thank Dr. Alan Cheville for mentoring me and giving me the opportunity to perform this project. I have learned a lot about science and myself through this degree.

I would like to thank Helen Daggs for going the extra mile, for me and all her students.

I would like to thank Barbara Caldwell for always having a smile ready when I needed it.

I would like to thank Nicholas Oswald for showing me the ropes in the THz lab and for working with me through this degree.

I would like to thank Suchitra Reiten and Kyrus Kuplicki for the endless stream of technical advice and for the camaraderie that made the long days in the office bearable.

I would like to thank Sree Harsha and Mufi Gong for being quick to offer both technical advice and a couch.

I would like to acknowledge Walmart Inc. and Greyhound Bus Line for their part in my graduate degree. It would have been far more difficult without the services they provide.

I would like to give special thanks to my parents for letting me take advantage of them, their home, their car, and their fridge. They always show more faith in me then I deserve.

But above all, I would like to thank my friend, editor, life coach, cheerleader, critic, and wife, Theresa. Who endured our time apart with more grace than a husband could ask for. Theresa, thank you for supporting me and letting me back into your life. It has been a long road, but we have made it here together. I thank the Lord for you and look forward to what the future will bring us.

TABLE OF CONTENTS

Chapter Page

LIST OF TABLES

Table Page

LIST OF FIGURES

Figure Page

Figure Page

CHAPTER I

INTRODUCTION

Terahertz (THz) radiation, also called far infrared radiation (FIR), allows observation of properties not visible with any other source of light. The application of THz radiation is at the heart of terahertz time domain spectroscopy (THz-TDS). THz-TDS functions by illuminating a material with a THz pulse and analyzing that material's frequency dependent characteristics. The coherent nature of this measurement makes it very sensitive, achieving signal to noise of 10000:1 [1]. These factors, combined with the table-top size of the apparatus, make THz-TDS a powerful scientific tool.

THz radiation is being applied to an ever increasing number of scientific fields. It was first created at IBM in the 1980's[2], making it a fairly recent science. As such, work is still being done to refine the technology behind making and detecting THz radiation. New applications for THz radiation are being developed as THz emitters and detectors become more reliable and powerful. Scanners for THz imaging are now being sold commercially [3], a cosmic THz detector will be installed in a new observatory in Antarctica [4], and THz radiation is being considered for safer airport security [5, 6]. However, THz-TDS remains the most widely used application of THz radiation. THz-TDS has found a home performing unprecedented sensing applications including measuring the high frequency

response of niobium superconductive transmission lines [7] and the coating thickness on pharmaceutical tablets [8], detecting cracks in space shuttle foam [9], identifying narcotics in opaque sealed envelopes [10] and conducting a host of chemical analysis. All of these capabilities are due to the molecular vibrations excited by THz radiation. THz-TDS plays an important role in science and will be the catalyst for future breakthroughs.

The objective of this research is to enhance THz pulses created in THz-TDS experiments by applying a layer of gold nanoparticles on the surface of the microchip. It is hypothesized that the nanoscale features of these gold particles will create regions of high electric field over the surface of the THz emitting microchip causing an increase in THz signal strength and bandwidth. In the course of this research, the effects of three types of gold nanoparticles were explored: gold black, colloidal gold and gold islands. These effects were determined by analyzing the THz pulses created from chips covered in varying amounts of these particles.

1.1 THz-TDS System

THz-TDS systems create and detect THz pulses. Different methods can be used to create the THz pulses. The two most popular methods use femtosecond laser pulses to short biased coplanar transmission lines or by creating a difference frequency through wave mixing laser pulses in a non-linear medium (called optical rectification) [11]. Lenses and parabolic mirrors collimate the created THz pulses and couple them to a receiving device. THz radiation is detected either through electro-optic sampling or measuring current flow across a receiving pair of coplanar transmission lines. The basic THz-TDS experimental

setup described by Martin [1] uses coplanar transmission lines for both transmission and reception. A beam splitter splits the laser pulses to gate both the receiving and transmitting lines. An optical delay line controls the timing of the laser pulses on the receiving line. The receiving lines, when gated, exhibit a slight bias voltage caused by the electric field of the detected THz pulse. This causes current flow across the receiver which is collected, amplified and recorded. Noise reduction in these systems is achieved with a lock-in-amplifier and optical chopper. Spectroscopy is performed on samples placed in the path of the THz radiation. Coherent THz pulses allow the sample's THz absorption coefficients and complex index of refraction to be measured. An example of a basic THz-TDS system is illustrated in Figure 1. Those interested in a more in-depth explanation of various the THz systems should refer to the review paper by Schmuttenmaer [11] and the Springer Handbook of Lasers and Optics, Chapter 17 [12].

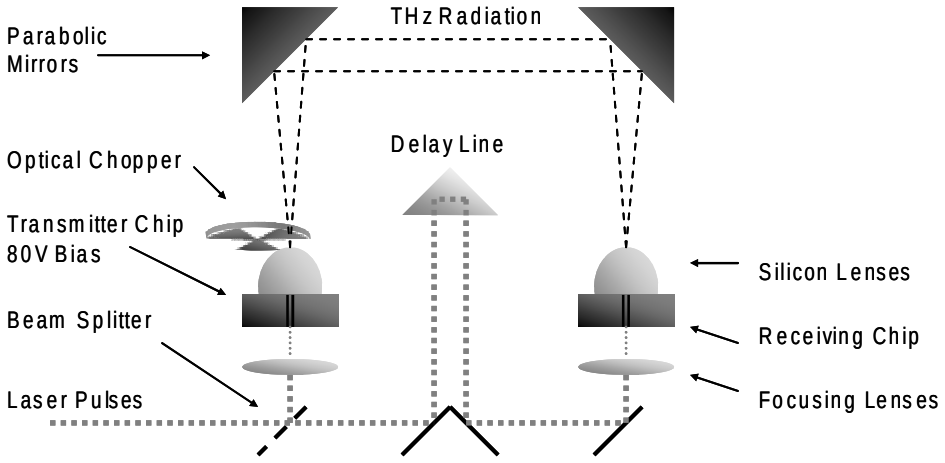

Figure 1: THz-TDS System

1.2 THz Coplanar Transmission Lines

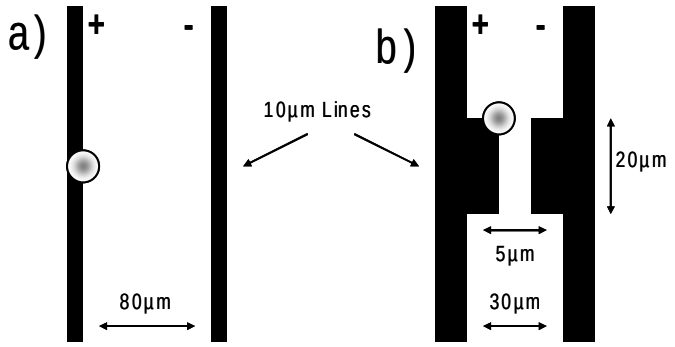

Figure 2: Transmission lines. a) Lines on the transmitter chip. b) Lines on the receiving chip. Circles indicate optimum placement of focused laser beam.

Coplanar transmission lines used for THz generation and detection have a relatively simple design. They are created with two metal lines spaced microns apart on a semiconducting substrate as seen in Figure 2. The metal lines are 5µm to 25µm wide, tens of millimeters long, and spaced 30µm to 80µm apart. Receiving lines and some transmission line designs have an additional antenna structure bridging across the lines. Transmission lines are biased by 60V to 80V. The optimum location to illuminate the lines is shown by the beam spot in Figure 2. As the laser beam focuses, the bandwidth and electric field strength of the resulting THz pulse increase. When the beam is focused, laser power must be limited to <20mW or risk damaging the transmission lines. The bias voltage creates an electrical field between the lines. A space-charge region next to the anode is created as electrons and holes are photogenerated into the system and because the barrier energy is low enough to stop positive charge build up against the cathode. When illuminated, optically injected carriers enhanced by the electric field accelerate across the lines creating a dipole antenna that emits radiation with THz frequencies [13]. This effect is strongest right next to the anode where the electric field is greatest. Pulse

magnitude and bandwidth are determined by the electron mobility and carrier life-time of the semiconductor [13]. The receiver is best illuminated at the corners of the bridging antenna structure connected to the anode. These corners follow the well-known property that sharp features build up excess charge. The receiver's substrate requires a very short carrier lifetime in order to capture the highest frequencies possible from the THz pulse. A THz transmitter and receiver are optimized or "peaked" when all further adjustment of the laser beam decreases the measured THz signal.

Although THz-TDS systems have a high signal to noise ratio, this ratio is still the limiting factor in many applications. THz transmitter design focuses on getting better signal to noise ratios by increasing pulse power. Early transmitters were designed like the receiver shown in Figure 2b [14] and made out of a very short carrier lifetime material called ion-implanted silicon on sapphire (SOS). SOS is still commonly used as the substrate in receiving lines. Gallium arsenide (GaAs) soon replaced SOS as the semiconductor in transmitters. It was found to increase the peak signal by a factor of 5 and to give an increase in bandwidth [15]. The metal transmission lines were also moved farther apart which let higher bias voltages be used. It was shown that THz pulse strength scaled with increasing voltage. This new THz transmission line design was called the gallium arsenide trap-enhanced field (GaAs-TEF) emitter [16]. The GaAs-TEF is currently the standard THz transmission line due to pulse power and cost. However, further improvements to these transmission lines were made by replacing the GaAs substrate with low-temperature-grown gallium arsenide (LT-GaAs). LT-GaAs makes the best THz transmission lines to date due to its fast recombination lifetime, high carrier mobility, and

high resistivity [17]. It can also absorb more laser power than GaAs without being damaged. Only its high cost and difficultly to manufacture consistently keep LT-GaAs from being commonly used. Better semiconductor substrates and transmission line designs have contributed to more powerful THz pulses.

1.3 Lithographic enhancement

Lithographically created sharp features on a THz transmission line can also create more powerful THz pulses by creating electric field singularities on the surface of a THz emitter. Work done by Cai [18] used a LT-GaAs substrate with a bridged antenna structure (similar to Figure 2b, and labeled FF in Figure 3) having a 90μm gap and 190μm distance between lines. The beam was focused to a spot size of ≈0.7μm. This experiment showed a three-fold THz field enhancement at the corners of the antenna structure over the common THz transmission line design with no bridging structure (Figure 2a). Further work by Cai [19] used an antenna structure with a 60μm line distance, 5μm distance gap, and a tightly focused 0.4μm diameter beam. This work found that sharp features on the transmission lines gave THz pulse enhancement, as seen in Figure 3. The greatest enhancement came from the feature labeled TT0 which gave more than double the THz power seen from the feature label FF. It is interesting to note this work also reports 40% more THz signal detected when these sharp features are used on a THz receiver.

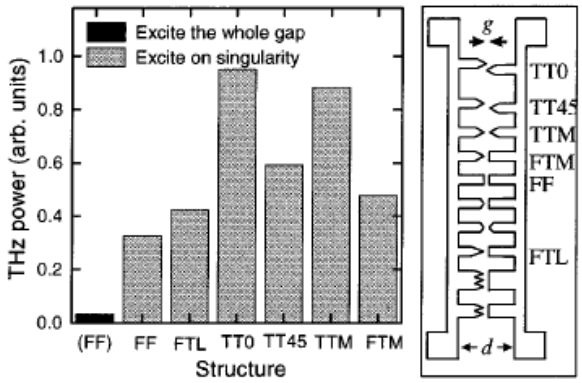

Figure 3: This shows sharp features (TT0) give a signal improvement over flat structures (FF). Various other shaped are compared. Lines have a 60μm distance (d), a, 5μm gap (g), 20V bias, and are illuminated with 20mW of laser power. Copied from [19].

Cai [19] showed that changes in the metal transmission lines could enhance THz signals. These changes are small compared to improvements gained through better semiconductor substrates, greater bias voltage, or more optical power. However, it is useful because other enhancement mechanisms are easily maximized. It is also worth noting that more THz enhancement could be gained if sharper features than those allowed through conventional lithography could be created, such as through nanoparticle deposition. The sharp features explored by Cai have not been widely adopted because the cost of creating new lithographic masks in most applications does not justify the small enhancement. This research seeks to create a similar THz signal enhancement, but one that does not require new lithography masks and can be added to pre-existing GaAs-TEF transmission lines.

1.4 Nanoparticle enhancement

Nanoparticles have unique properties that can improve THz signals. The best example of this is LT-GaAs, which gets its properties from arsenic nanoparticles that precipitate out of the GaAs structure [20]. The chemical and electrical properties of nanoparticles can be

changed according to particle size, shape, and dispersion. Arsenic particles in LT-GaAs have uniform diameters between ≈5nm to ≈90nm [20]. They become evenly scattered throughout the substrate during the creation of LT-GaAs. Changing the size of the arsenic particles varies the properties of the material. These particles give LT-GaAs its high electron mobility and short carrier lifetime. Nanoparticles are responsible for the superior properties of this semiconductor.

This research seeks to create a cost effective improvement to THz transmitters by depositing gold nanoparticles on the surface of a THz transmitter. Gold was selected because it has high conductivity, is resistant to oxidation, and can form a variety of nanoscale structures. Gold nanoparticles can enhance the electric fields which create THz pulses by creating points of high voltage across the lines. Nanoparticles are small enough that they can create sharper features than are possible through standard lithography techniques [18]. These particles can create areas of high voltage at locations where these particles make contact with the transmission lines and are well separated from other nanoparticles. This locally improves the DC electric field without risking chip damage caused by increased bias voltage. Three types of gold nanoparticles, each with a different structure, were selected to test this enhancement. It is unknown what structure would be the most effective. The selected gold nanoparticles are gold black, colloidal gold, and gold islands. Nanoparticles deposited on the surface of a THz emitter could possibly give enhancement without etching the transmitter, changing the transmitter's semiconductor substrate or creating new lithography masks. Nanoparticles could theoretically create

stronger THz pulses on coplanar transmission lines, with a low investment of time and material.

An additional mechanism of electric field enhancement caused by metal nanoparticles was observed in work performed by Fedorovich [21]. This work found "hot spots" of high voltage that formed as current percolated across metal island films. One hot spot was created per percolation path and each was intense enough to reshape the metal islands around it. Much of the energy in this "hot spot" was in the form of heat, but it also was in the form of emitted electrons and photons. IR illumination was also shown to cause this effect provided it had intensity greater than $10^4 W/cm^2$. This work was performed on a number of metals including gold. Gold nanoparticles could use this effect to inject photon and electrons into the substrate of the THz emitter.

1.5 Gold black

Gold black is the first type of gold nanoparticle chosen for this experiment. Gold black is a type of metal smoke [22] and looks like soot. It is a porous particulate made of pure gold that is black to dark reddish brown in color. Work by Harris [23] detailed its creation and optical properties. It is of interest because it retains the thermal and electrical properties of gold, but has good IR absorption properties. For a thickness between 3 to 8μm its reflectance at visible and IR wavelength has been measured at <0.3% [24]. It is also an ultra light material with a density between 50 to 100$\mu g/cm^2$ [24]. Gold black can retain it shape when floated off a glass surface and will turn from black to brown in color if crushed [25]. It is created by evaporating gold in a low-pressure inert atmosphere [23].

In this environment, gold atoms collide with gas particles, lose their energy and form aggregates with other gold atoms in the air [26]. These aggregates eventually settle on a surface and bind with other aggregates they encounter. These aggregates exhibit fractal geometry [27]. Individual particles in this network are from 10nm to 20nm in diameter [23]. The optical properties of gold black come from their small particle size and fractal structure [28-30]. This structure governs the allowed plasmon oscillations in the gold black. When crushed, the structure is destroyed and other plasmon oscillations appear, as evident by a reddish color change. A sample of gold black can be seen in Figure 4 and Figure 5. Deposition of gold black on the surface of the THz transmitter will absorb a fraction of the incident light. This research will show if the structure of gold black will cause observable field enhancement across a THz emitter.

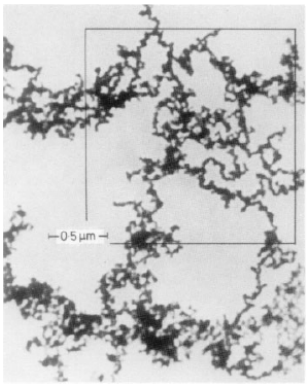

Figure 4: Fractal structure of gold black can be seen. Copied from [26].

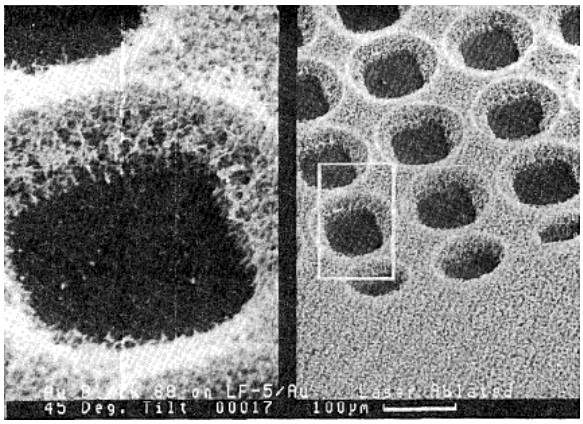

Figure 5: Porous nature layer of gold black is visible. Holes were created through laser ablation. Copied from [24].

1.6 Colloidal Gold

The second type of nanoparticle deposited in this experiment was colloidal gold. There are many types of gold colloids, but the one chosen for this work is a gold hydrosol created from sodium citrate reduced in chlorauric acid. Detailed research on the creation and optical properties of this colloid was performed by Turkevich [31]. The optical properties of colloidal gold are evident in its ruby-red color. The color of colloidal gold correlates to the size of the gold particles suspended in the solution. Particle size governs plasmon oscillations which absorb light at selected wavelengths. The red color comes from 20nm gold particles with a blue shift occurring as the particles become larger. When making the colloidal gold solution, particles up to 160nm in diameter can be selected by adjusting the reagents and the rates at which they are combined [31] [32]. Beyond this, the solution becomes unstable and flocculation occurs. Gold particles are formed when gold atoms are release from the chlorauric acid, creating large, unstable gold particle aggregates. These aggregates soon break down into smaller, denser, and more stable gold particles. Citrate ions remain bonded to the gold through this process and collect around the newly formed gold nanoparticles. This creates electrostatic repulsion that keeps the

particles dispersed in the solution [33]. This process can be observed in a newly created batch of colloidal gold. Over a few minutes the solution changes through an array of colors: colorless, black, purple, blue and, depending on the final particle size, red. When allowed to evaporate, colloidal gold hydrosols collapse down and reveal fractal networks [34]. These networks are black in color with sharp features the same size as the particles in the colloid. But by adjusting how the colloidal was created, the minimum feature size (smallest particle size) can be controlled. This research will show if this fractal structure will cause observable field enhancement across a THz emitter.

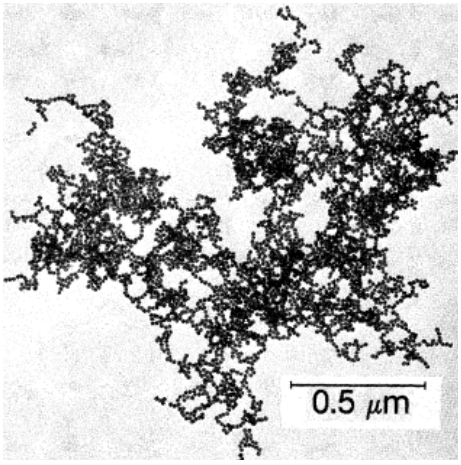

Figure 6: Fractal structure of colloidal gold can be seen. Copied from [34].

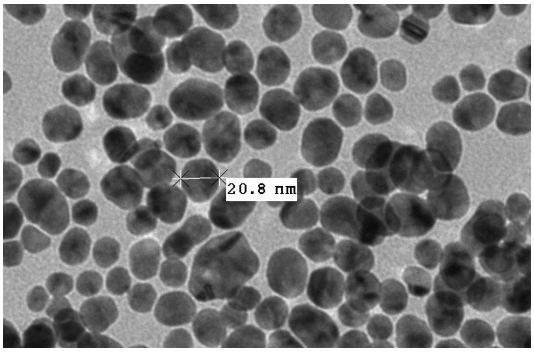

Figure 7: Colloidal gold particles seen under a TEM. These particles were created with the same methodology and reagents as the ones created for this research. Copied from [35].

1.7 Gold Islands

The last type of nanoparticle to be deposited in this experiment was gold islands. It has been known for decades that a thin layer of gold deposited in high vacuum creates granulates or islands before forming a continuous metal surface [22]. Gold islands differ from the other two types of nanoparticles in this research in that they are not fractal structures, but are a collection of separated randomly assembled nanometer groups. Deposition rate and annealing can alter the dimensions of these gold islands [36, 37]. Gold deposited to a 5nm layer, as read by a quartz thickness monitor, at a rate of 0.03nm/s, showed islands 20nm across with 4nm to 10nm spacing between islands [38] [37]. This can be seen in Figure 8a. Work done at a slower deposition rate of $8x10^{-4}$ nm/s deposited a 3nm layer with islands 4nm across [39]. Gold island particles start to coalesce as the gold layer gets thicker. This thickness is called the percolation threshold. When this happens the resistance of the gold layer drops four orders of magnitude [40]. The percolation threshold is at 6nm for gold islands and at 20nm the gold islands are one continuous sheet [38]. This is important on a THz transmitter where the transmission lines would short if the gold island layer became too conductive. This research will show if the structure of gold island particles will cause observable field enhancement across a THz emitters.

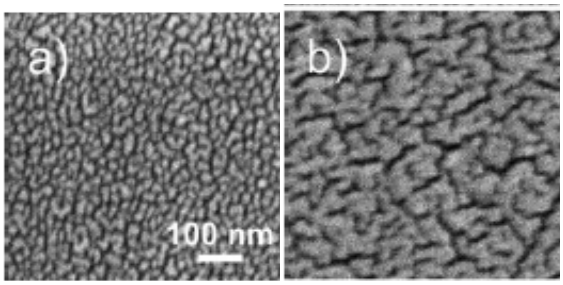

Figure 8: Gold island particles. a) Shows a 4nm gold layer. Discrete islands can be seen. b) Shows a 8nm gold layer. This layer crosses the percolation threshold, gold islands are now connected. Copied from [38].

1.8 Conclusion

This research seeks to expand the capabilities of currently used THz-TDS systems by enhancing the surface electric field on THz transmitters with gold nanoparticles. The unique structure of gold black, colloidal gold, and gold islands would create regions of high voltage on the emitter improving the quality of generated THz pulses. If similar results to those found with lithographically created sharp features were observed this effect could obtain double the maximum THz signal. The aim of this work is to discover if enhancement of this magnitude will occur. Optimization of this process will be saved for future work. A standard THz-TDS experimental setup, as described in Chapter 2, will be used to collect THz pulse data. The resulting pulses, along with any other observations and measurements, will be listed in Chapter 3. This data will be discussed and analyzed in Chapter 4. Chapter 5 will summarize the findings of this work and suggest future avenues of research.

CHAPTER II

METHODOLOGY

Exploring the effect of nanoparticles on THz pulses required the construction of a THz-TDS system and samples of nanoparticles. This chapter explains the methodology used to build this system and collect data. Equipment used to construct the THz-TDS system is described, including parts, operations, and innovations. The THz transmitter, chip and housing designs are given followed by sample THz data. Deposition techniques for gold black, colloidal gold and gold islands were adapted to available equipment using preliminary data. Deposition techniques are explained as well as the measurements taken at each step of sample preparation.

2.1 THz-TDS Experimental Setup

The THz-TDS system used in this experiment is based on the system used by Martin [1]. A Kapteyn-Murnane Labratories Ti:Sapphire IR pulse laser with a 86MHz repetition rate was used as the laser source. Gold coplanar transmission lines located in the transmitter of the system were fabricated on a gallium arsenide (GaAs) chip. The transmitter consisted of one GaAs chip, a plano-convex 15mm focal length lens used to focus the laser to the surface of the chip, and a truncated ball lens 6.437mm tall with a 5mm radius made of high resistivity silicon used to collimate the emitted THz radiation. The GaAs

chip and Si ball lens were housed in X Y translators, while the 15mm lens was mounted on a Z axis translator. The receiver, made with aluminum lines on a silicon-on-sapphire (SOS) semiconductor, was housed in a similar device. The transmitter and receiver were located at the 11.5cm focus of two parabolic mirrors. This created a symmetric optical system. This system is shown in Figure 1. The laser pulses were split at a Coherent Pellicle beam splitter rated at 40/60 for 800nm light. One beam traveled through a delay line composed of a mirror mounted on a National Aperture MM-4M-F-50 linear stage. This was driven by a National Aperture MicroMini Controller at an average scan speed of 48μm/s. The power to the transmitter was supplied by a GWInstek DC power supply that could limit both the voltage and current supplied to the transmitter chip. Noise reduction was achieved by using a Thor Labs Model1000 Optical Chopper operated between 287MHz and 329MHz and connected to a Model SR830 DSP Lock-In Amplifier. The amplifier modulated the THz pulses at a low frequency (MHz) rate and then subtracted out any electrical signal, like random noise, which was not modulated at this same rate. The lock-in amplifier used an integration time constant of 100ms for all THz scans. The current collected from the receiver chip was amplified by an Ithaco model 564 current amplifier biased by an Intelitender 15V battery. To measure and automate the experiment, Labview version 7.1 was used on a Gateway model # E-1600 D computer connected serially to the motor controller and lock in amplifier. These components are similar to those used in other THz-TDS systems and allow for high quality data collection.

This system used a National Aperture MicroMini Controller and motorized stage to replace a Newport UTS100CC Linear Stage and Newport MM3000 Motion Controller. The National Aperture devices cost $3000 [41] [42] less than the Newport components. However, they only had a resolution of 1.24μm, while the Newport devices had a resolution of 0.1μm. The low resolution of the National Aperture devices made it impossible to get the precise steps between data points required to complete a Fourier transform. To overcome this limitation, a continuous scanning method was developed for the National Aperture stage. The scan was purposely over sampled and then a MATLAB algorithm was written to linearly interpolate the scan and to acquire data at the desired resolution. For this THz data, exactly 5μm between data points gave adequate frequency bandwidth. This innovation added value to the laboratory used for this work.

2.2 THz Transmitter Design

The THz transmitters used in these experiments include not only the transmission lines on GaAs chips but also the stages, lens, and electrical contacts that house the chip. The entire transmitter unit had to be redesigned due to the number of chips scanned in succession. All other available THz transmitters had chips permanently mounted in place. To facilitate moving chips in and out of the transmitter unit, first an aluminum connector block was machined on which the transmitter's X Y stages and a magnetic base were mounted. This block was machined to tight tolerances to limit movement of the stages each time they were replaced. The magnetic base allowed the entire unit to be removed and replaced in the THz-TDS system without changing alignment. Next, Macor (ceramic) disks were fabricated that could be fastened with a retaining inside an X and Y stage.

Macor was selected because it is nonconductive, machineable, and will not flex. THz chips could be mounted with Norland optical adhesive to the back of these disks. The disks could be quickly switched in and out of the X Y stage. Pins mounted on a circular circuit board were also placed in the X Y stage. They extended through holes in the Macor disk and established electrical contact with the THz chip. Lines on the chip could be switched on and off with dipswitches mounted on a second circuit located outside the unit connected by a ribbon cable. This design is shown in Figure 9. This design made chips easily removable and maintained the original alignment to within 50µm. But small errors in chip timing (when the pulses hit the chip) and chip rotation were introduced with this design. The system operator could restore the correct pulse timing after a new chip was installed by moving the delay line a small amount until the signal was maximized again. Chip rotation error was eliminated by creating a reference transmission line on each chip. Also differences in alignment between chips where reduced with the use of a reference line. Using a reference line and this new transmitter design made scanning multiple chips effective and accurate.

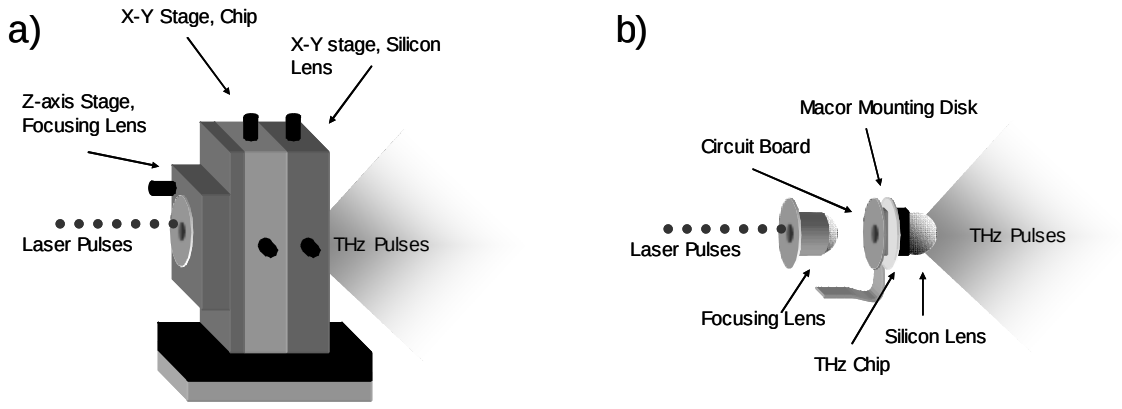

Figure 9: THz transmitter. a) Outside. b) Inside.

THz transmissions lines were fabricated from gold evaporated on a GaAs wafer and later cut in to $1cm^2$ chips. The chips were created following lithographic, etching, and dicing instructions provided by Dr. Weili Zhang [43]. The GaAs wafers were purchased from Photo Sciences Inc. and each wafer made +30 chips. Each chip had four transmission lines on it. The reference and sample lines required only two lines. The dimensions of a single transmission line was 9mm x 10µm with 80µm separating each pair of lines, as shown in Figure 10. $1mm^2$ gold pads at the end of each line made electrical contact with the power supply through pins on the circular circuit board. Current was generally kept below 4mA and was never allowed to exceed 8mA.

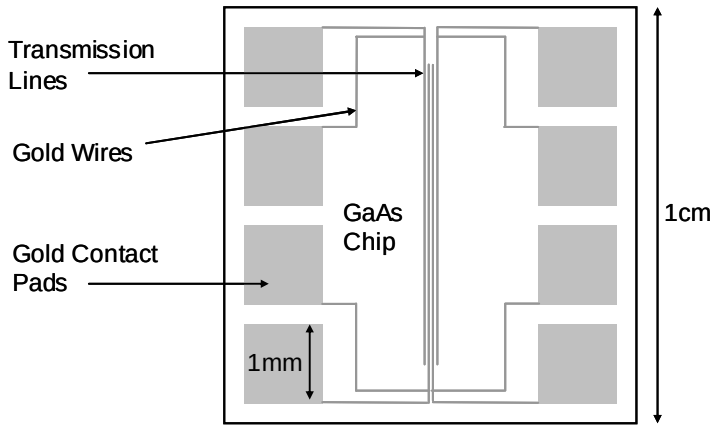

Figure 10: GaAs Chips used to create THz radiation

Cleaning each chip was very important to ensure good nanoparticle adhesion and uniform electrical properties. Oils and material >1µm would show up visually in a microscope. These could be best cleaned off with methanol and acetone applied with lens paper or a Q-tip. Care had to be taken using a Q-tip because the transmission lines could easily be wiped off the chip. 30 seconds immersed in acetone using a Cole-Parme 8892 sonic bath machine would remove particles, as well as, 2 minutes of plasma cleaning using 200V of

argon and hydrogen in a MARCH Inc. plasma cleaner. Electrical tests on cleaned chip showed that these cleaning procedures were effective.

2.3 THz Pulse Measurements

THz pulses were traced out as the delay lined scanned over the duration of the pulse. Each scan took about 5 minutes. A sample THz pulse with its corresponding frequency spectra created through a Fourier transform is shown in Figure 11. This THz pulse was sent though humid air to show THz water absorption. The undulations shown after the time domain pulse are ringing caused by the vibration of water molecules. These create molecular specific absorption lines in the frequency spectra of Figure 11. Scans are always taken in <%5 relative humidity to atmosphere to reduce absorption from water vapor. An important characteristic of this pulse is the height of the time domain pulse. This corresponds to the maximum strength of the THz signal. The integration of the frequency spectra indicates pulse power. The full width half maximum (FWHM) can be seen from the frequency spectrum as well as bandwidth. Scan length corresponds to frequency resolution which is 22GHz for these scans. If need be, zero padding can be used to artificially improve frequency resolution. The goal of these experiments is to improve the signal strength and the bandwidth relative to the reference pulse.

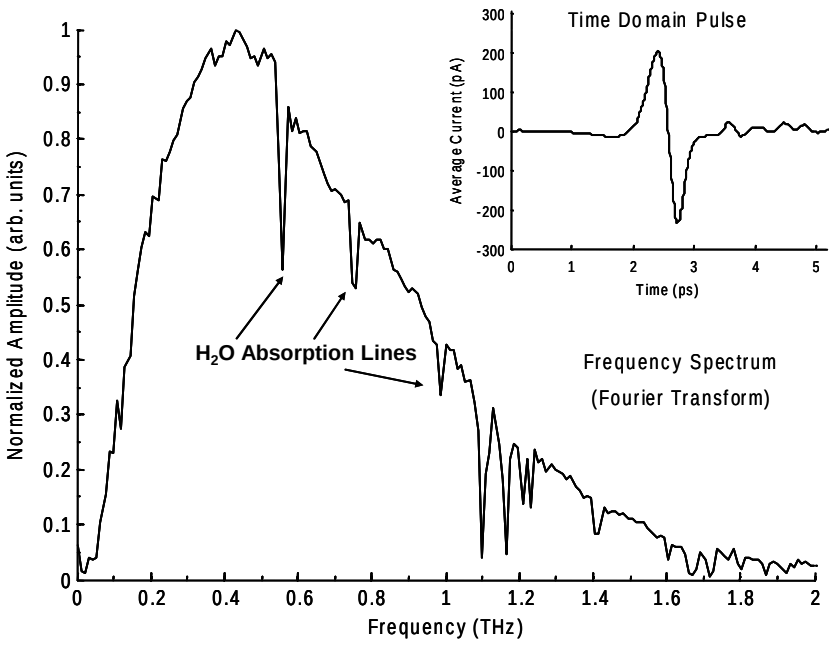

Figure 11: Frequency and time domain THz pulse.

2.4 Additional Measurements

Measurements of the electrical characteristics of the chips were taken before and after the chips were placed in the THz-TDS system. This recorded their electrical characteristics with and without laser illumination. Current and voltage (IV) curves on dark THz chips were measured in a HP 4145B Semiconductor Parameter Analyzer from 0V to 100V with the current limited to 0.4mA or 4mA. This device could reliably measure currents as low as 1nA. Resistance values calculated from these currents had an upper limit of ≈50GΩ. Chips illuminated with the laser beam had IV curves measured at discrete points in the THz-TDS system after it had been well aligned.

Many features on the coplanar transmission lines could be resolved optically. Particle density, coverage area and sometimes particle size could be determined from optical inspection. A Nikon Eclipse L150 microscope was used to take images of the chips after

cleaning and deposition. Optical inspection was used to gauge if particle deposition was effective and to observe its structure. Damaged lines could also be observed with the microscope. It was an invaluable tool in preparing the chips and analyzing particle deposition.

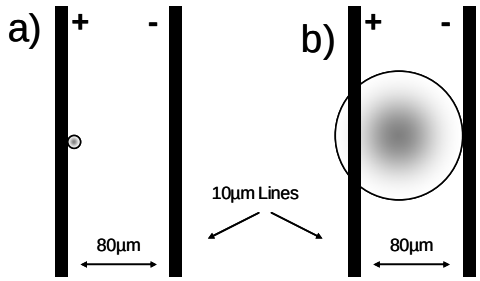

Figure 12: Spot size of the laser beam. At focus a) ≈ 4μm and defocused b) ≈ 80μm.

Additional THz data was taken with the laser beam defocused. This departs from the standard THz-TDS system which uses a focused laser beam. Preliminary data indicated that the THz signal was stronger when a larger spot size was used. It showed that an additional signal maximum was reached when the beam size was increased from focus (≈ 4μm) to spanning the transmission lines (≈ 80μm), as shown in Figure 12. These tests will show if a large beam size makes a difference on the nanoparticle deposited THz emitters. Further measurements were taken by increasing incident laser beam power on these emitters. These tests explore additional scenarios in which these particles could be advantages to THz pulse generation.

2.5 Gold Black Deposition

Gold black deposition followed the procedure described in Harris [25] [23] with some equipment adaptations. An Edwards Auto 306 thermal evaporator was loaded with a R.D. Mathis Company tungsten boat filled with approximately 0.1g of 99.995% pure gold

powder and mounted between the evaporator's high power electrodes. The sample was mounted close (27mm) to the boat for maximum effect due to the mean free path of 0.1mm at a pressure of 3.3mbar for gold atoms in a nitrogen atmosphere. To accomplish this, a shutter was removed and the sample mounted in its place. This served the dual purpose of having the sample close enough for gold black deposition and controlling the amount of gold black deposited. When the shutter was opened the sample would move away from the boat. In addition, an aluminum shield was placed on the edge of the sample to further block particles when the shutter was open. This was stupendous at controlling the deposited gold black. Conductivity tests showed no gold black was deposited with an open shutter.

The gold was heated with a current of 40A in a 3.3mbar nitrogen atmosphere containing 99.995% pure nitrogen gas. In this environment the gold evaporated, as described in Chapter 1, and collected on the sample. The current was kept constant during deposition so gold black thickness only depended on deposition time. No cooling system could be created for the evaporator so heat was managed by depositing for 30sec and then allowing the chamber to cool for 1min. Heat was further removed by using the aluminum mount as a heat sink. Deposition results were observed optically and electrically. Care had to be taken during this process to seal the thermal evaporator chamber and burn off excess oxygen for a few minutes prior to deposition, as described by Louis Harris [25]. This prevented the formation of tungsten trioxide along with the gold black, which appeared as a blue layer in the chamber and turned transparent when exposed to air. Tungsten trioxide combines with the gold atoms and creates a composite material called

type II gold black or gold smoke filters [44] [25]. After deposition, the reference line on each chip was created by carefully removing the gold black with a dry Q-tip guided by a razor blade positioned ≈0.25mm above the chip.

2.6 Colloidal Gold Deposition

Colloidal Gold was created following the procedure described in Turkevich [31]. A smaller amount was created for these experiments. It was created by heating 55mL of chlorauric acid until boiling then adding 5.5mL of 1% sodium citrate solution while stirring. Once the sodium citrate was added the solution underwent several color changes over the course of a few minutes. The final color reached by this solution was violet, corresponding to 50nm particles [32]. This procedure was shown to be very sensitive to slight variations in the reagents. Preliminary results found that colloidal gold created without ultra high purity DI water (≈18MΩ resistively) was unstable and the gold immediately precipitated out of solution. Care had to be taken to thoroughly clean the glassware using the highest purity DI water before contacting the colloidal gold. Sample variability was reduced by using colloidal gold samples that all came from a single solution.

A Finnpipette from Thermo Labsystems was used to deposit one 1μL drop of colloidal gold on the THz chips. Originally a Laurell 400 Spinner set at 3000rpm was also used to deposite several drops, but optical results showed no visible layer of particulate to form even after fifty 40μL drops were deposited. Electrical results showed only a small increase in current across the lines after this large deposition. Also no indication of fractal

network formation was observed. Room temperature evaporation was then tried. It was found that this created large fractal networks of gold particles. The gold particles created aggregates large enough to be seen optically (≈1μm diameter) and had noticeably changed the electrical properties of the line. These particles were most likely caused by aggregation of smaller particles during evaporation of the water. Room temperature evaporation also deposited extra salts that grew into crystals as the water in the solution evaporated. These salts were dissolved with DI water leaving randomly located holes in the fractal network. Colloidal gold was placed on the GaAs chips after creating a watertight seal by masking one of the lines with scotch tape. The gold particles were thickest near the edge of a drop and were deposited with the edge of a drop near the center of the transmission line.

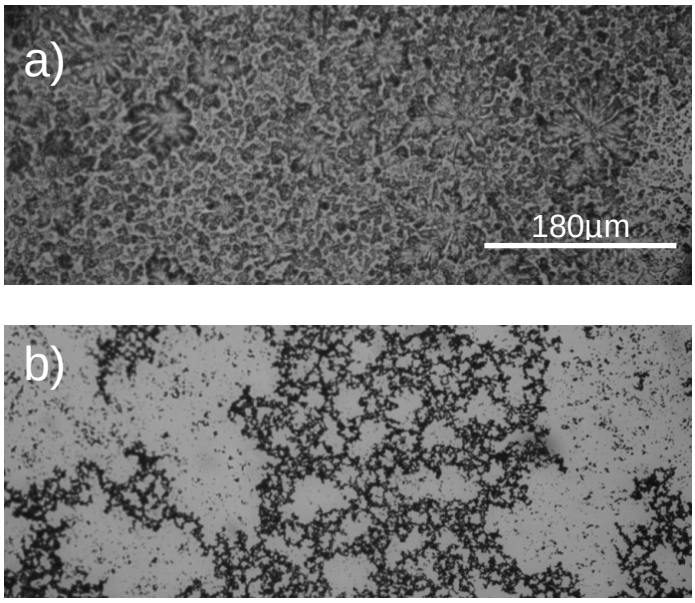

Figure 13: Colloidal gold deposited through room temperature evaporation. a) Shows salt crystal growth. b) Shows the gold fractal networks revealed after DI water dissolved the salt crystals.

2.7 Gold Island Deposition

Gold islands were deposited with a tungsten boat containing ≈0.1g of 99.99% pure gold powder using an Edwards Auto 306 thermal evaporator in an $x10^{-5}$ mbar vacuum at a rate of ≈0.05nm/s. This method took advantage of the phenomenon that evaporated gold will aggregate into islands before making a continuous surface. This layer must be below the percolation threshold of ≈6nm [38] so the gold will not make a continuous layer and short the transmission lines. At this rate of evaporation, Osawa measured the largest IR absorption to occur close to the percolation threshold [36]. Measurements of gold thickness were performed with a thickness monitor containing a Maxtek 6MHz crystal sensor placed inside the evaporator. This monitor had been calibrated to be accurate to within 0.1nm of the layer's thickness. A reference line was made by masking one line with aluminum foil prior to being loaded in the evaporator. Chips were mounted on an aluminum plate attached to the thickness monitor to give the most accurate reading.

2.8 THz System Alignment

THz-TDS system alignment is the single largest source of error in a THz system. Alignment requires monitoring the peak THz signal while adjusting by hand several optical components. Much of the system alignment was performed before measurements were taken and then remain untouched including aligning the receiver, parabolic mirrors and optics guiding the IR beam. The IR beam at focus made a micron sized a spot so precise positioning of the optics was required. When all these components are correctly positioned the signal is "peaked" or optimized, meaning further movement of optical

components only lessens the signal. This ensured that THz-TDS system remained the same for each chip scanned.

After the system was optimized, only the transmitter unit needed to be adjusted each time a new chip was used. This required adjusting the lens on the Z translator stage used to change laser focus, the X Y stage that holds the GaAs THz chip, and the X Y stage that holds the silicon lens. Once the system was again optimized the following process was followed to move between the sample and reference line:

1. The bias voltage on the first line was lowered.
2. The first line was switched off and the second line was switched on.
3. The bias voltage was increased again to the same level as the previous line
4. The X Y stage was slowly turned in the Y direction toward the second line, until the THz signal returns.
5. The signal was optimized in the Y direction on the stage.
6. The X and Y directions of the Si lens was slightly adjusted to compensate for the movement across the chip.
7. Repeat steps 5 and 6 until the chip is optimized.

Only the transmitter was touched while moving from one line to the next. Also the focus on the Z translation stage and the X direction of the X Y stages were never touched in this process. Also this method caused the Si lens to remain stationary with respect to the optical spot. This method limited the number of uncontrolled variables introduced between the sample and reference lines.

Each measured pulse had a corresponding reference pulse. This virtually eliminated variability between chips. However, slight variability still existed between the reference and sample lines on each individual chip. For this work, signal increases greater than 10% over the reference pulse are considered beyond the range of uncontrollable alignment errors. But signal increases of 100% over the reference pulse (double) are the desired levels of enhancement. Smaller gains will require further analysis to verify and may not be significant enough to merit further investigation. Comparing the maximum signals from the sample and reference lines will show the level of signal gain or loss caused by each nanoparticle deposition.

2.9 Conclusion

Building a system that could take this THz data was a challenging process. It required adapting a complex THz-TDS system to scan multiple chips while maintaining as much of the original alignment as possible. Accuracy of the data was maintained by using a reference line. This gave each sample its own baseline to compare too and minimized alignment differences between chips. Repeatable methods of depositing the three nanoparticles on one of the four transmission lines were developed. This required adaptation of the nanoparticle creation processes, modification of equipment and nondestructively masking each GaAs THz chip. The equipment and techniques developed as part of this methodology will give accurate THz data.

CHAPTER III

THZ NANOPARTICLE DATA

The finished THz-TDS system was used to record data for THz transmitters covered in gold black, colloidal gold and gold island nanoparticles. This data showed how pulse characteristics were affected by these particles. Nine chips in total were scanned in the THz-TDS system, each with varying amounts of gold nanoparticle deposited on them. Gold black deposition was measured in seconds of deposition time. Three chips were deposited with 100 seconds, 300 seconds, and 1000 seconds of gold black. Colloidal gold was measured in amount of concentration compared to the original concentration of the colloid. Three chips were deposited with $1/16^{th}$ concentration, $1/4^{th}$ concentration, and an undiluted concentration of colloidal gold. Gold island particles were measured by the amount of gold deposited on the chips. Three chips were deposited with 1nm, 3nm, and a 5nm layer of gold island particles. Data on many of these chips was taken with a defocused laser beam to observe if increasing the area of interaction between the beam and nanoparticles affect the THz pulse. Reflectivity data on the gold island layers was also collected. Additional high power laser beam data was collected from the 3nm gold island chip after it appeared to create stronger THz pulses when laser power was varied. The recorded THz data explored the range of effects these nanoparticles had on GaAs THz emitters. This data is displayed below.

3.1 Gold Black Data

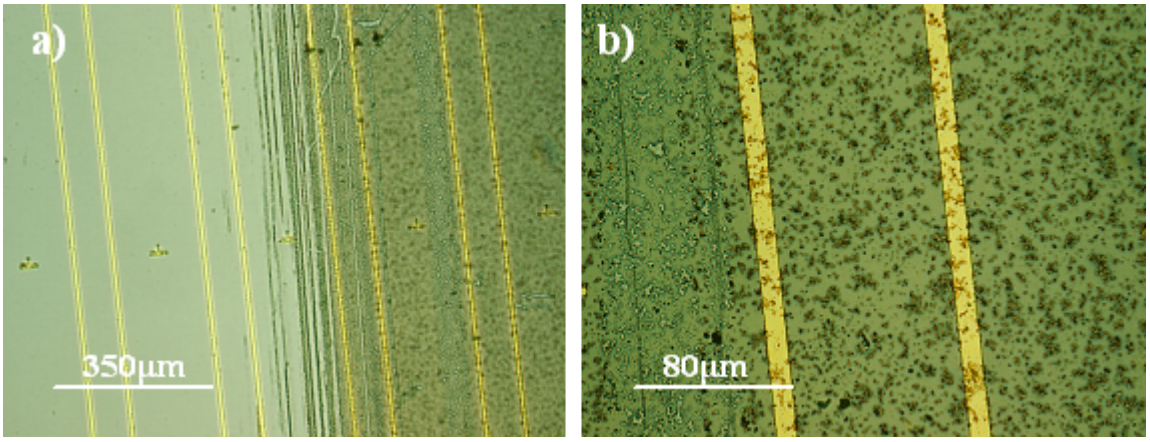

Figure 14: 100 seconds of gold black deposition. a) x10 magnification shows reference line on the far left and sample line on the far right. b) x50 magnification of the sample line.

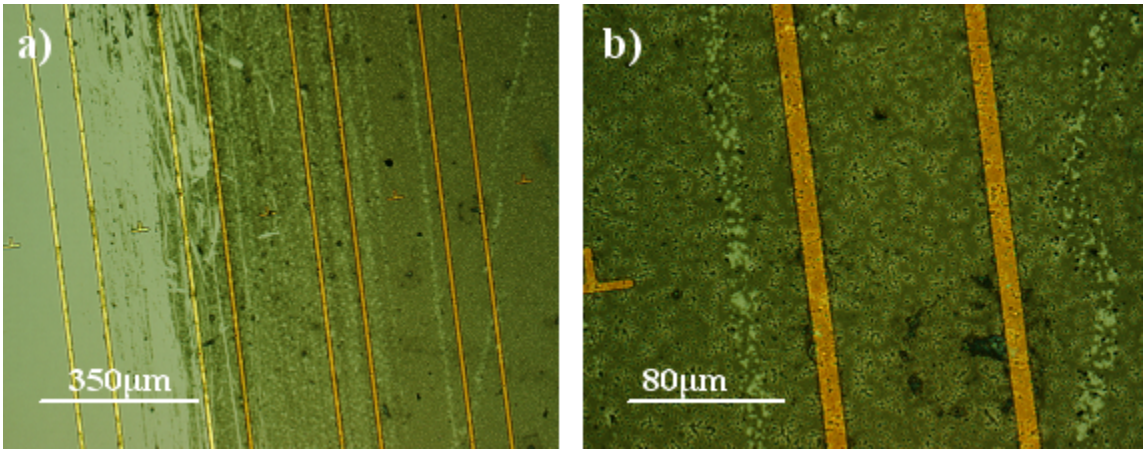

Figure 15: 300 seconds of gold black deposition. a) x10 magnification shows reference line on the far left and sample line on the far right. b) x50 magnification of the sample line.

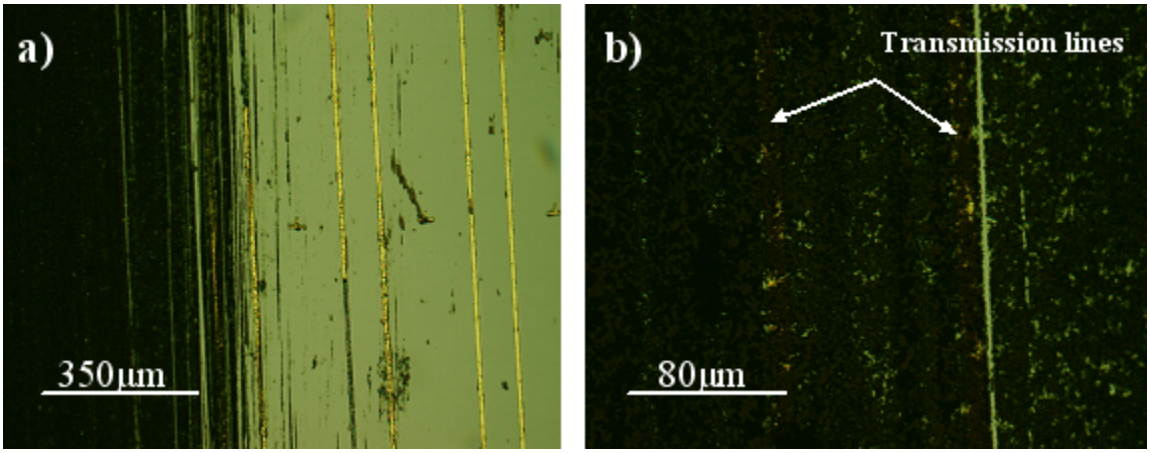

Figure 16: 1000 seconds of gold black deposition. a) x10 magnification shows reference line on the far right and sample line on the far left. b) x50 magnification of the sample line.

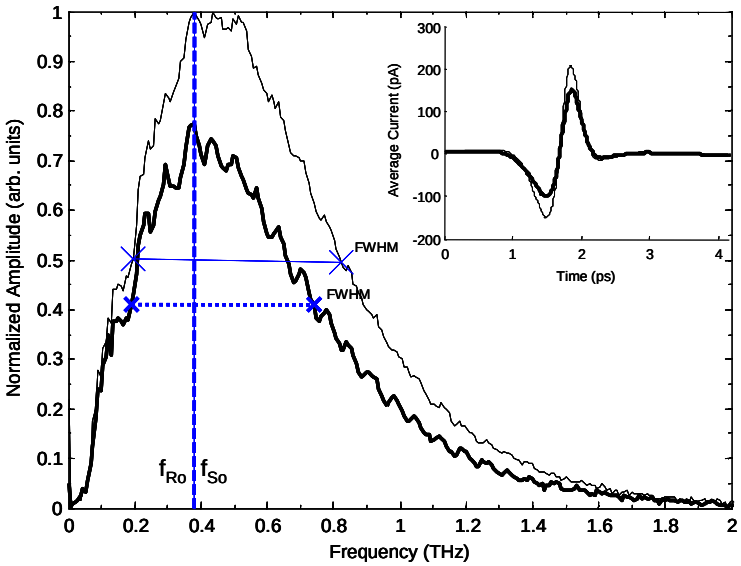

Figure 17: THz pulse from 100 seconds of gold black deposition. Sample is in bold. Sample pulse was biased at 31V with 2mA across the chip. Ref. pulse was biased at 31V with 3mA across the chip. Oscillations in the spectra are an artifact of alignment.

	Reference	Sample	Δ =(S - R)
Max signal	200 pA	150 pA	-50 pA
Center Frequency	0.4 THz	0.4 THz	NA
Normalized Integrated Amp.	1.0	0.7	-0.3
FWHM	0.6 THz	0.6 THz	NA

Table 1: Data collected from Figure 17.

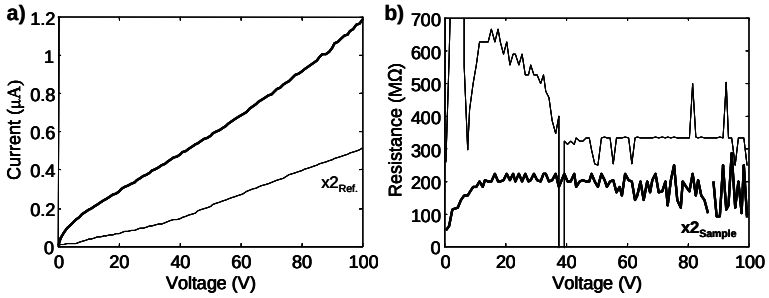

Figure 18: a) VI curve across the above chip in darkness. b) Resulting resistance from that curve.

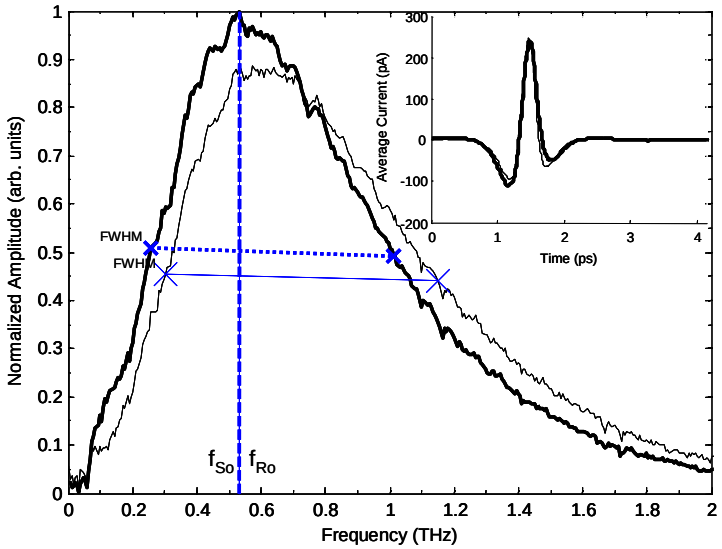

Figure 19: THz pulse from 300 seconds of gold black deposition. Sample is in bold. Sample pulse was biased at 30V with 1mA across the chip. Ref. pulse was biased at 30V with 0.4mA across the chip.

	Reference	Sample	Δ =(S - R)
Max signal	250 pA	240 pA	-10 pA
Center Frequency	0.5 THz	0.5 THz	NA
Normalized Integrated Amp.	1.0	1.0	NA
FWHM	0.8 THz	0.8 THz	NA

Table 2: Data collected from Figure 19.

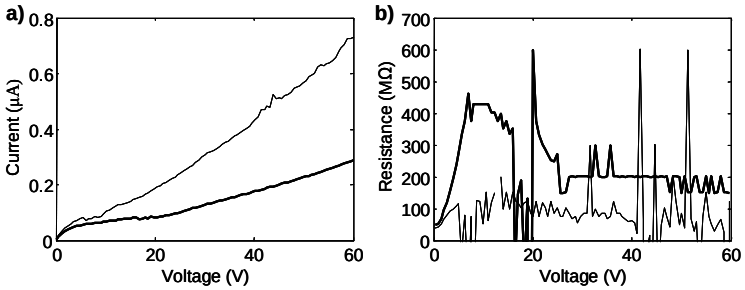

Figure 20: a) IV curve across the above chip in darkness. b) Resulting resistance from that curve.

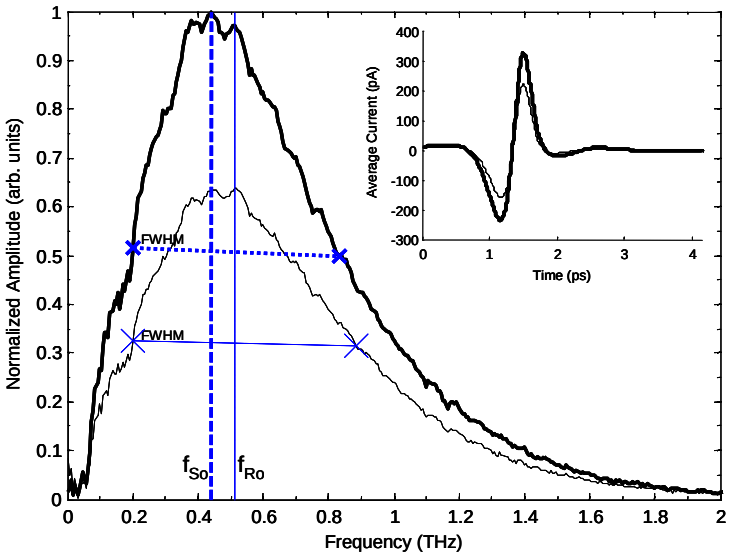

Figure 21: THz pulse from 300 seconds of gold black deposition with a defocused laser beam. Sample is in bold. Sample pulse was biased at 30V with 3mA across the chip. Ref. pulse was biased at 30V with 2mA across the chip.

	Reference	Sample	Δ =(S - R)
Max signal	210 pA	320 pA	110 pA
Center Frequency	0.5 THz	0.4 THz	-0.1 THz
Normalized Integrated Amp.	0.7	1.0	0.3
FWHM	0.7 THz	0.6 THz	-0.1 THz

Table 3: Data collected from Figure 21.

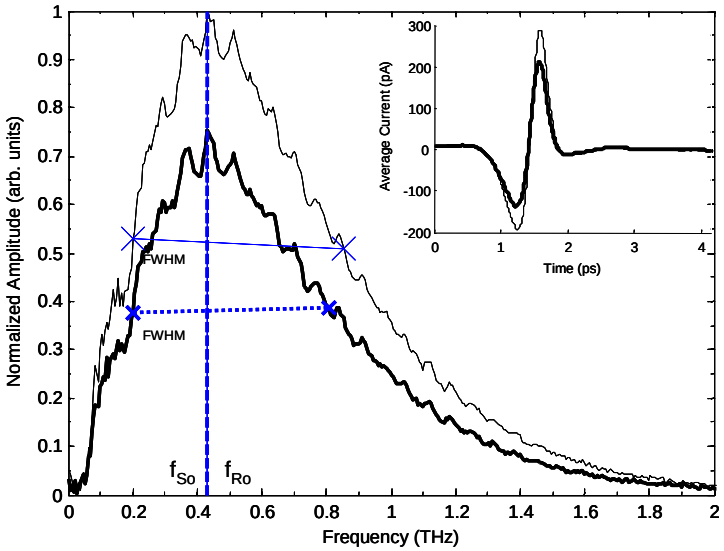

Figure 22: THz pulse from 1000 seconds of gold black deposition. Sample is in bold. Sample pulse was biased at 30V with 2mA across the chip. Ref. pulse was biased at 30V with 3mA across the chip. Oscillations in the spectra are an artifact of alignment.

	Reference	Sample	Δ =(S - R)
Max signal	290 pA	210 pA	-80 pA
Center Frequency	0.4 THz	0.4 THz	NA
Normalized Integrated Amp.	1.0	0.7	-0.3
FWHM	0.7 THz	0.6 THz	-0.1 THz

Table 4: Data collected from Figure 22.

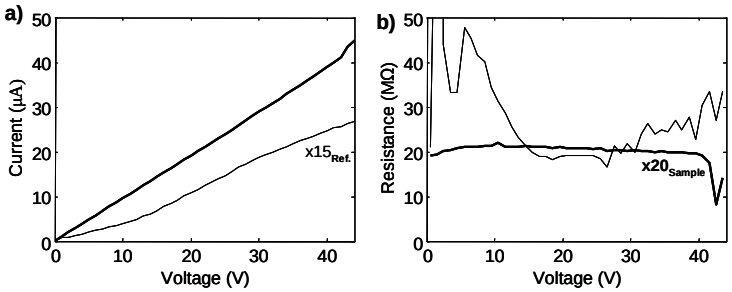

Figure 23: a) IV curve across the above chip in darkness. b) Resulting resistance from that curve. Current across sample line rose sharply at 45V.

3.2 Colloidal Gold Data

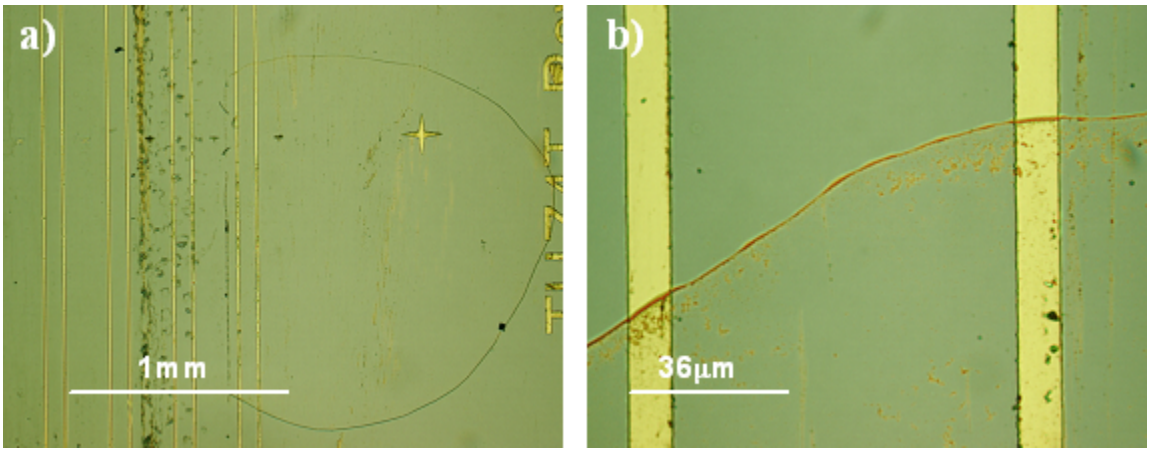

Figure 24: 1µL colloidal gold mixed with 93.75% DI water. a) x5 magnification shows the reference line on the far left and the sample line partially covered by a colloidal gold drop on the far right. b) x100 magnification of the sample line showing the edge of the drop across this lines and gold particles below it.

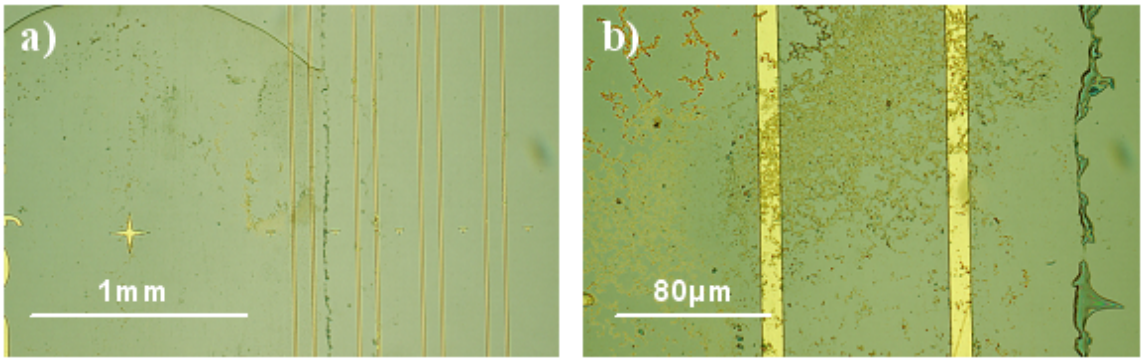

Figure 25: 1µL colloidal gold mixed with 75% DI water. a) x5 magnification shows the reference line on the far right and the sample line partially covered by a colloidal gold drop on the far left. b) x50 magnification of the sample lines in the middle of the drop.

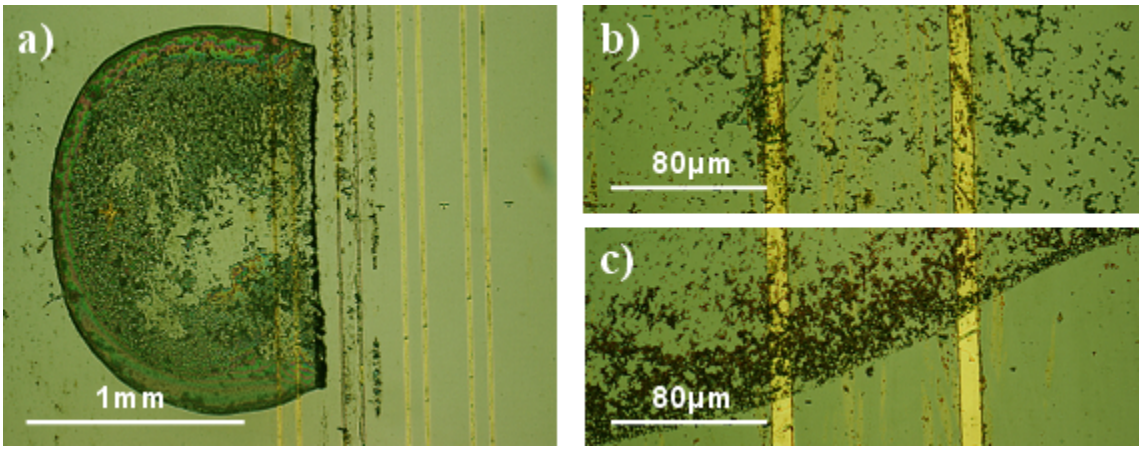

Figure 26: 1µL colloidal gold. a) x5 magnification shows the reference line on the far right and the sample line partially covered by a colloidal gold drop on the far left. b) x50 magnification of the sample lines in the middle of the drop. c) x50 magnification of the sample lines at the edge of the drop

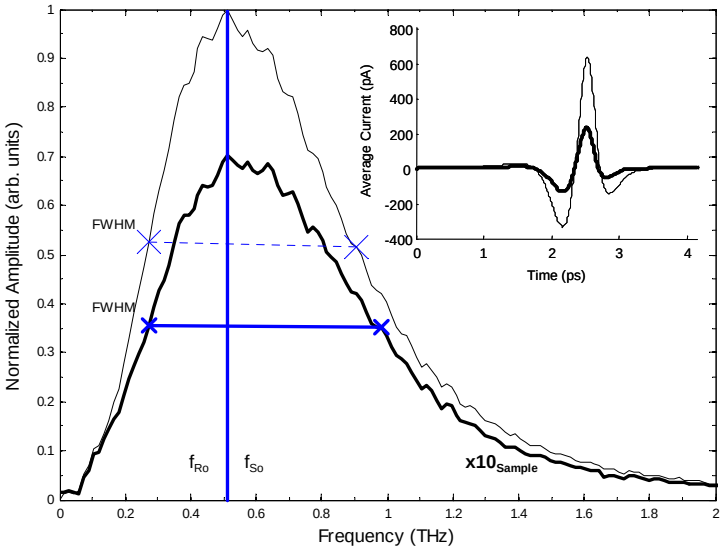

Figure 27: THz pulse from 1/16th solution Colloidal Gold. Sample is in bold. Sample pulse was biased at 30V with 3.95mA across the chip. Ref. pulse was biased at 30V with 2.07mA across the chip.

	Reference	Sample	Δ =(S - R)
Max signal	640 pA	230 pA	-410 pA
Center Frequency	0.5 THz	0.5 THz	NA
Normalized Integrated Amp.	1.0	0.4	-0.6
FWHM	0.6 THz	0.7 THz	0.1 THz

Table 5: Data collected from Figure 27.

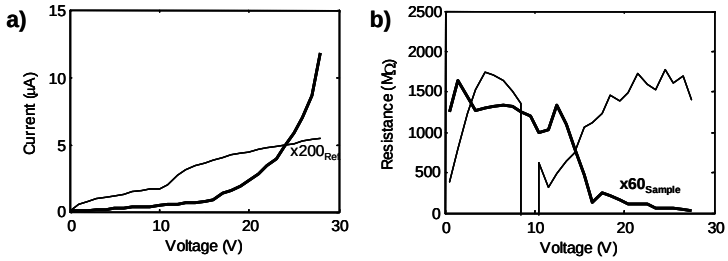

Figure 28: a) IV curve from the above chip in darkness. Current on the sample line sharply increases at 30V. b) Resulting resistance from that curve.

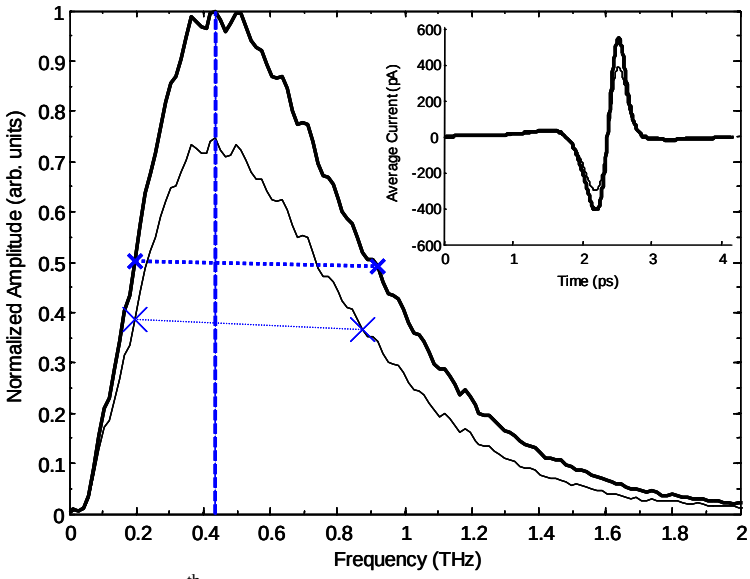

Figure 29: THz pulse from 1/16th solution colloidal gold using a defocused laser beam. Sample is in bold. Sample pulse was biased at 32.24V with 5.16mA across the chip. Ref. pulse was biased at 32.26V with 2.88mA across the chip.

	Reference	Sample	Δ =(S - R)
Max signal	390 pA	550 pA	160 pA
Center Frequency	0.4 THz	0.4 THz	NA
Normalized Integrated Amp.	0.7	1.0	0.3
FWHM	0.7 THz	0.7 THz	NA

Table 6: Data collected from Figure 29.

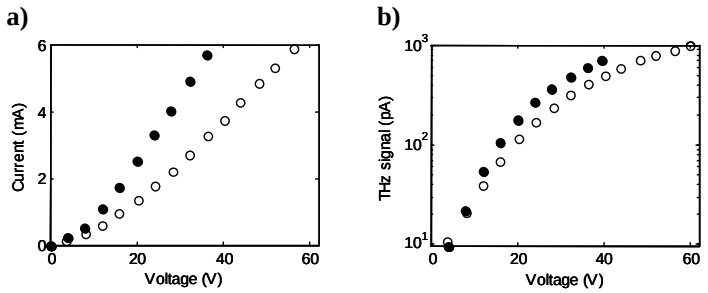

Figure 30: a) IV curve from the above chip with 16.8mW laser illumination. c) Resulting THz signal as a function of voltage, limited at 6mA and 60V.

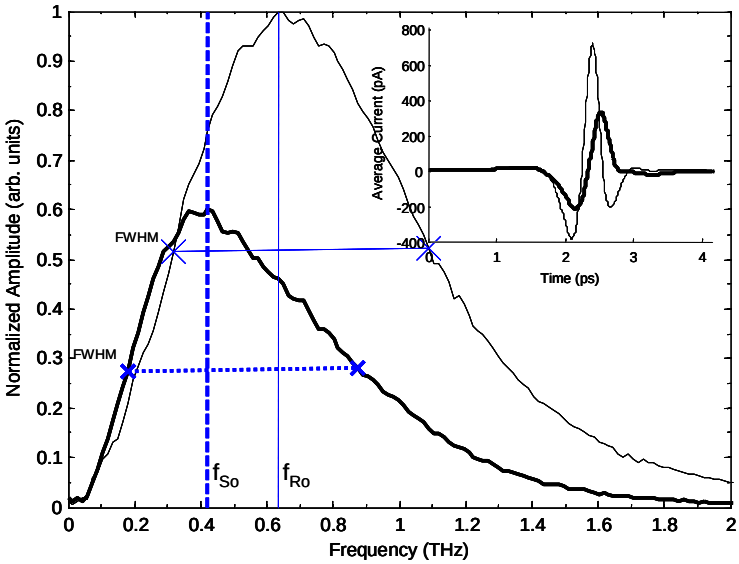

Figure 31: THz pulse from 1/4th solution of colloidal gold. Sample is in bold. Sample pulse was biased at 52.8V with 5.33mA across the chip. Ref. pulse was biased at 52.2V with 1.88mA across the chip

	Reference	Sample	Δ =(S - R)
Max signal	710 pA	330 pA	-380 pA
Center Frequency	0.6 THz	0.4 THz	-0.2 THz
Normalized Integrated Amp.	1.0	0.5	-0.5
FWHM	0.8 THz	0.7 THz	-0.1 THz

Table 7: Data collected from Figure 31.

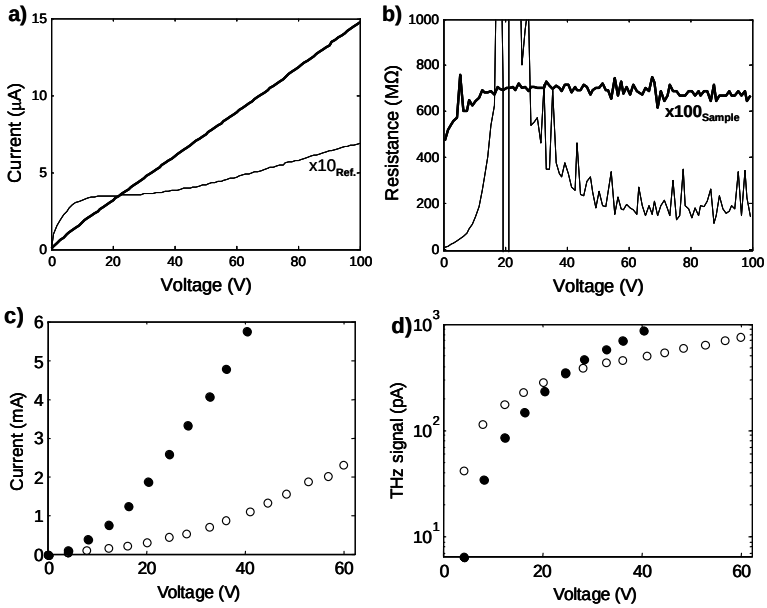

Figure 32: a) IV curve from the above chip in darkness. b) Resulting resistance from that curve. c) IV curve from the above chip with 16.8mW laser illumination. d) Resulting THz signal as a function of voltage, limited at 6mA and 60V.

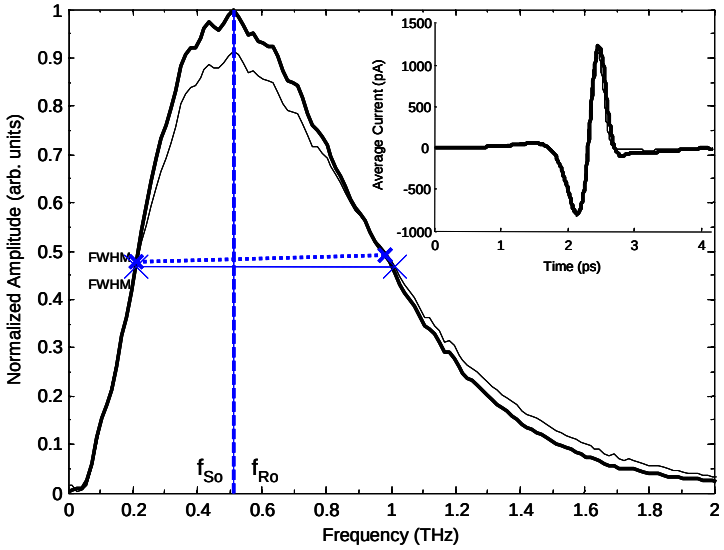

Figure 33: THz pulse from 1/4th solution colloidal gold using a defocused laser beam. Sample is in bold. Sample pulse was biased at 43.8V with 6.55mA across the chip. Ref. pulse was biased at 52.3V with 4.45mA across the chip.

	Reference	Sample	Δ =(S - R)
Max signal	1150 pA	1240 pA	90 pA
Center Frequency	0.5 THz	0.5 THz	NA
Normalized Integrated Amp.	1.0	1.0	NA
FWHM	0.8 THz	0.8 THz	NA

Table 8: Data collected from Figure 33.

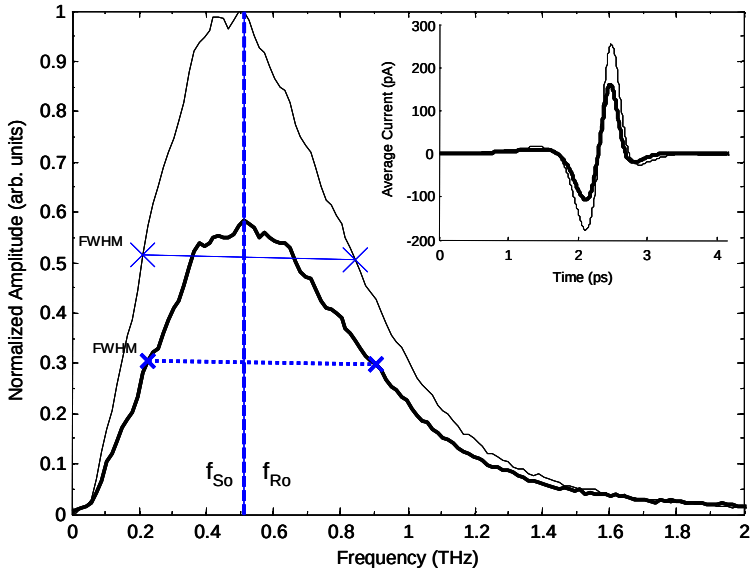

Figure 34: THz pulse from 1µL drop undiluted colloidal gold solution. Sample is in bold. Sample pulse was biased at 20.43V with 6.27mA across the chip. Ref. pulse was biased at 20.43V with 2.39mA across the chip.

	Reference	Sample	Δ =(S - R)
Max signal	250 pA	160 pA	-90 pA
Center Frequency	0.5 THz	0.5 THz	NA
Normalized Integrated Amp.	1.0	0.6	-0.4
FWHM	0.6 THz	0.7 THz	0.1 THz

Table 9: Data collected from Figure 34.

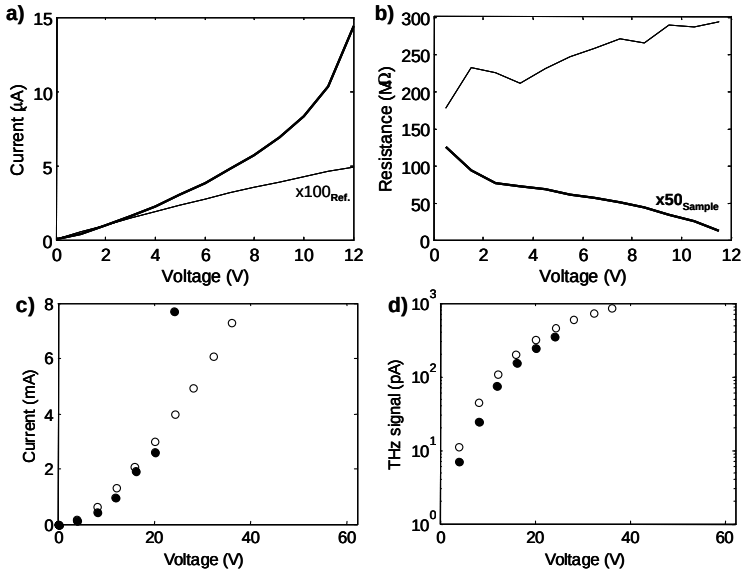

Figure 35: a) IV curve from the above chip in darkness. Current on the sample line sharply increases at 13V. b) Resulting resistance from that curve. c) IV curve from the above chip with 16.8mW laser illumination. d) Resulting THz signal as a function of voltage, limited at 6mA and 60V. The sample line current goes beyond 6mA at 20V.

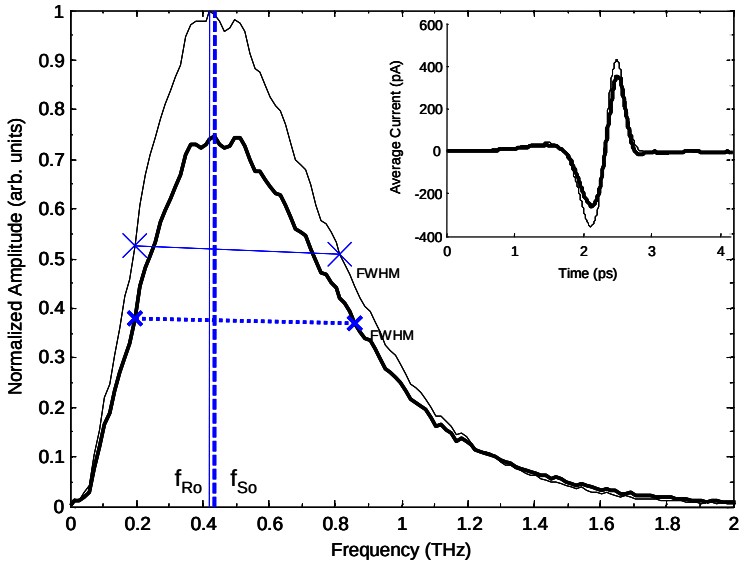

Figure 36: THz pulse from 1µL drop undiluted colloidal gold solution using a defocused laser beam. Sample is in bold. Sample pulse was biased at 20.43V with 8.16mA across the chip. Ref. pulse was biased at 20.49V with 2.98mA across the chip.

	Reference	Sample	Δ =(S - R)
Max signal	430 pA	350 pA	-80 pA
Center Frequency	0.4 THz	0.4 THz	NA
Normalized Integrated Amp.	1.0	0.8	-0.2
FWHM	0.7 THz	0.7 THz	NA

Table 10: Data collected from Figure 36.

3.3 Gold Island Data

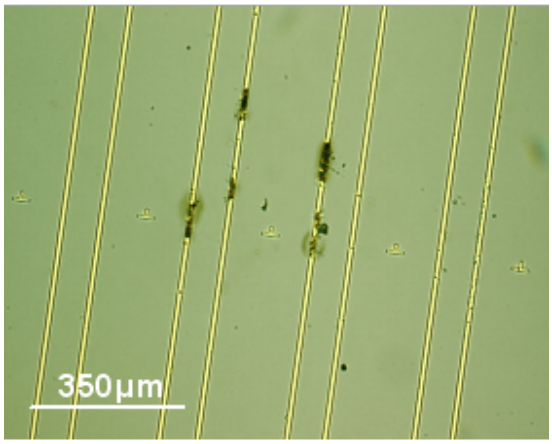

Figure 37: 1nm gold islands at x10 magnification. The sample line located at the far right is visually indistinguishable from the other lines on the transmitter.

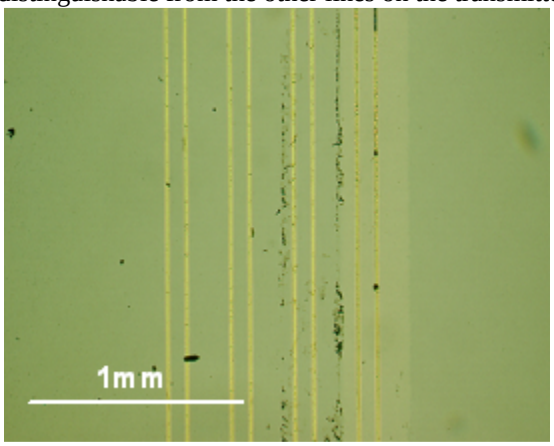

Figure 38: 3nm gold islands at x5 magnification. A visible bright band is across the sample line at the far right. The reference line is at the far left.

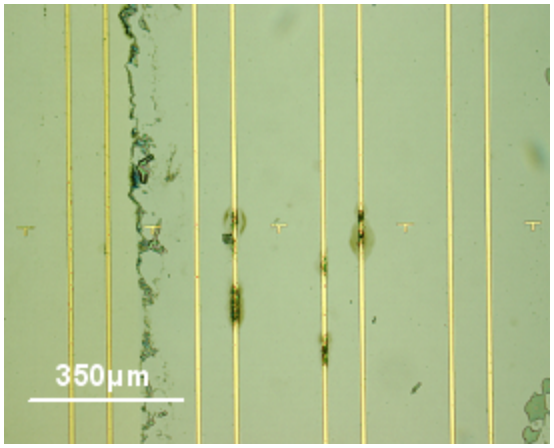

Figure 39: 5nm gold island particles at x10 magnification. Discoloration is visible on the gold island line at the far left. The reference line is at the far right.

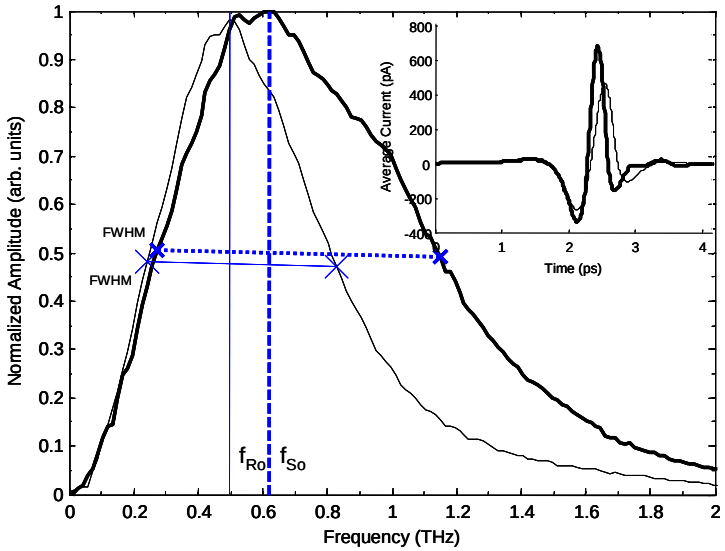

Figure 40: THz pulse from 1nm gold island deposition. Sample is in bold. Sample pulse was biased at 45.1V with 4.37mA across the chip. Ref. pulse was biased at 45.0V with 2.07mA across the chip.

	Reference	Sample	Δ =(S - R)
Max signal	460 pA	680 pA	220 pA
Center Frequency	0.5 THz	0.6 THz	0.1 THz
Normalized Integrated Amp.	0.7	1.0	0.3
FWHM	0.6 THz	0.9 THz	0.3 THz

Table 11: Data collected from Figure 40.

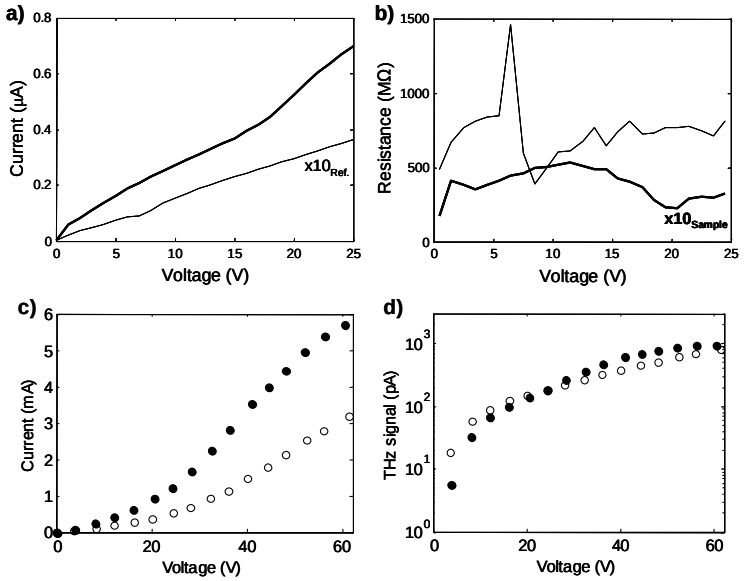

Figure 41: a) IV curve from the above chip in darkness. Current on the sample line sharply increases at 28V. b) Resulting resistance from that curve. c) IV curve from the above chip with 16.8mW laser illumination. d) Resulting THz signal as a function of voltage, limited at 6mA and 60V.

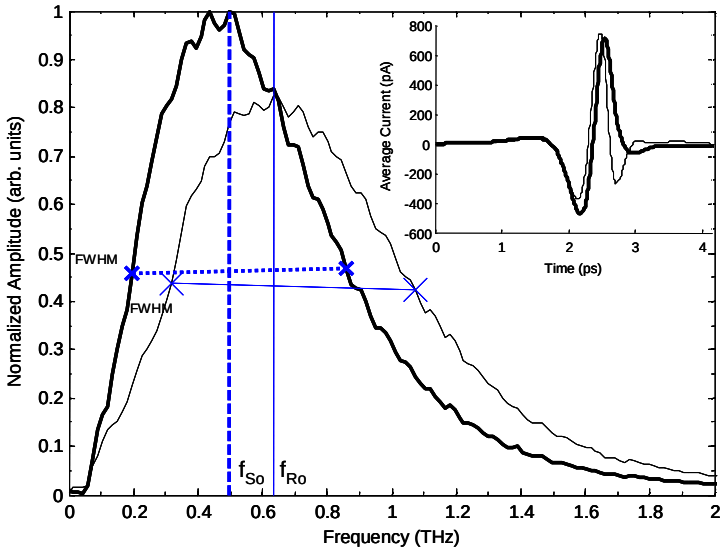

Figure 42: THz pulse from 3nm of gold island deposition. Sample is in bold. Sample pulse was biased at 61.2V with 5.90mA across the chip. Ref. pulse was biased at 51.4V with 2.53mA across the chip.

	Reference	Sample	Δ =(S - R)
Max signal	740 pA	710 pA	-30 pA
Center Frequency	0.6 THz	0.5 THz	-0.1 THz
Normalized Integrated Amp.	1.0	1.0	0.0
FWHM	0.8 THz	0.7 THz	-0.1 THz

Table 12: Data collected from Figure 42.

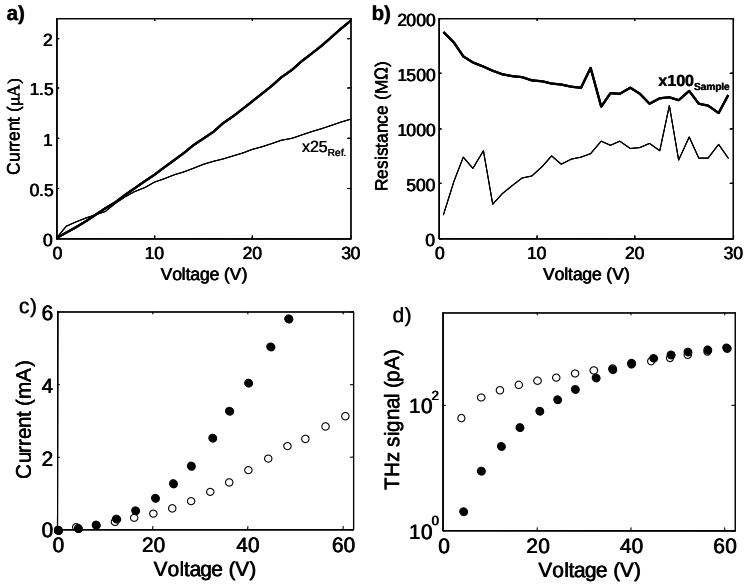

Figure 43: a) IV curve from the above chip in darkness. Current on the sample line sharply increases at 30V. b) Resulting resistance from that curve. c) IV curve from the above chip with 16.8mW laser illumination. d) Resulting THz signal as a function of voltage, limited at 6mA and 60V.

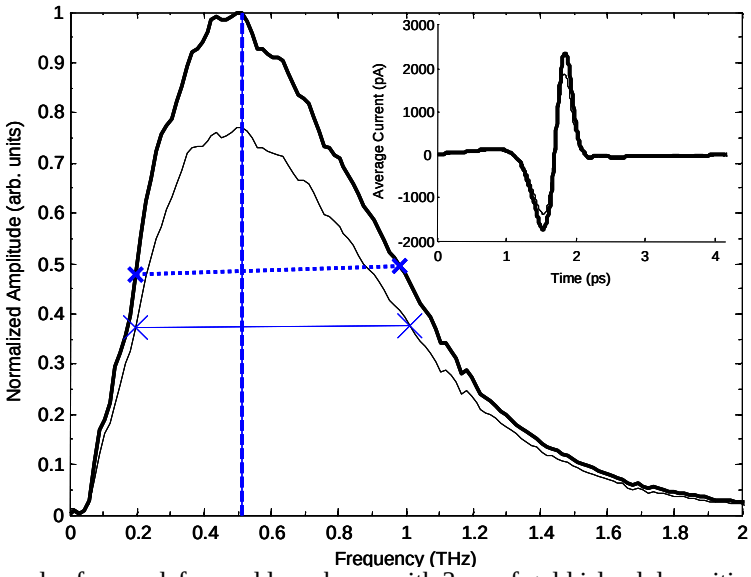

Figure 44: THz pulse from a defocused laser beam with 3nm of gold island deposition. Sample is in bold. Sample pulse was biased at 40.71V with 3.10mA across the chip. Ref. pulse was biased at 40.7V with 3.16mA across the chip.

	Reference	Sample	Δ =(S - R)
Max signal	1860 pA	2330 pA	470 pA
Center Frequency	0.5 THz	0.5 THz	NA
Normalized Integrated Amp.	0.8	1.0	0.2
FWHM	0.8 THz	0.8 THz	NA

Table 13: Data collected from Figure 44.

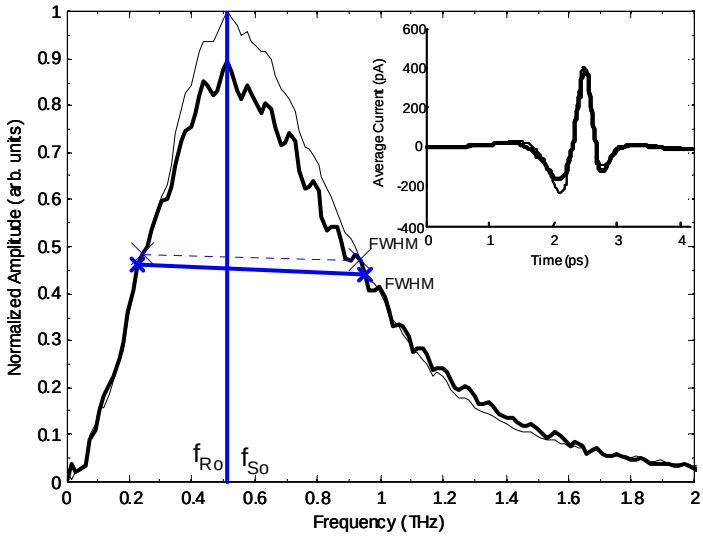

Figure 45: THz pulse 5nm of gold island deposition. Sample is in bold. Sample pulse was biased at 36.83V with 1.67mA across the chip. Ref. pulse was biased at 36.8V with 3.76mA across the chip. Oscillations in the spectra are an artifact of alignment.

	Reference	Sample	Δ =(S - R)
Max signal	400 pA	380 pA	-20 pA
Center Frequency	0.5 THz	0.5 THz	NA
Normalized Integrated Amp.	1.0	0.9	-0.1
FWHM	0.7 THz	0.7 THz	NA

Table 14: Data collected from Figure 45.

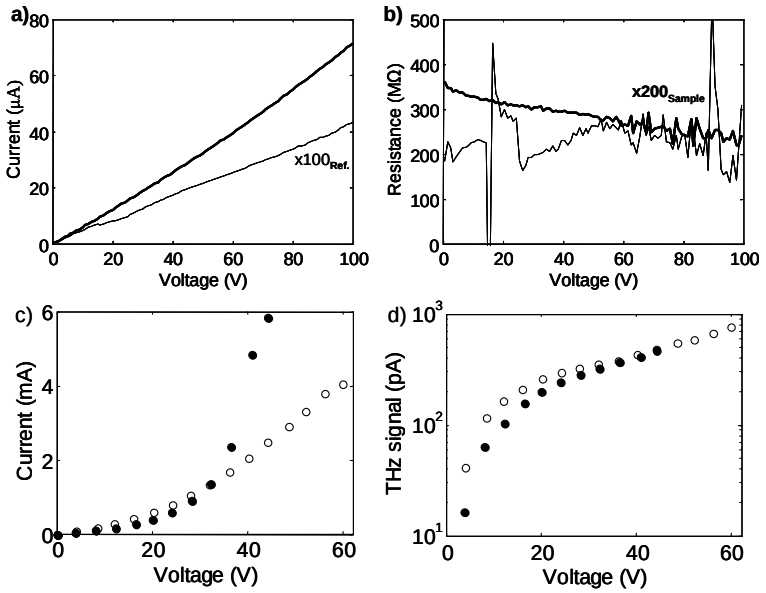

Figure 46: a) IV curve from the above chip in darkness. Current on the sample line sharply increases at 30V. b) Resulting resistance from that curve. c) IV curve from the above chip with 16.8mW laser illumination. d) Resulting THz signal as a function of voltage, limited at 6mA and 60V.

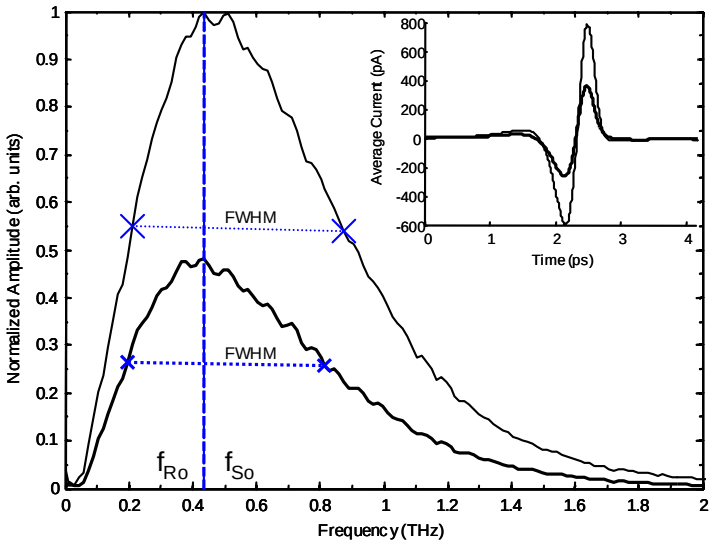

Figure 47: THz pulse from 5nm gold island deposition with a defocused laser beam. Sample is in bold. Sample pulse was biased at 36.83V with 3.04mA across the chip. Ref. pulse was biased at 36.8V with 3.74mA across the chip.

	Reference	Sample	Δ =(S - R)
Max signal	780 pA	360 pA	-420 pA
Center Frequency	0.4 THz	0.4 THz	NA
Normalized Integrated Amp.	1.0	0.5	-0.5
FWHM	0.7 THz	0.7 THz	NA

Table 15: Data collected from Figure 47.

3.4 Defocused High Power Data

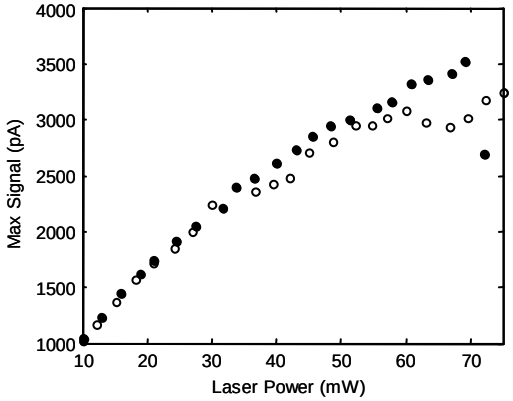

Figure 48: Plots of max THz signals for given laser beam powers. The laser beam was defocused to avoid chip damage. This data was taken on a chip deposited with 3nm of gold island particles at 40.8V and 2.48 for the sample line and 40.8V and 2.79mA for the reference line.

3.5 Gold Island Reflectivity

Gold Island Thickness	Reflectivity ~35º
0nm (Blank GaAs)	0.464
1nm	0.461
3nm	0.539
5nm	0.632

Table 16: Reflectivity of gold island particles on GaAs.

3.6 Conclusion

This data records the THz pulses created with transmitters covered in gold black, colloidal gold and gold island nanoparticles. Comparing each pulse to a reference pulse shows the changes caused by these particles. A quick look over the data shows that most pulses have characteristics similar to the reference pulse. As described earlier, small improvements in signal would be difficult to detect due to the inherent variability in the experimental system, but more importantly would not achieve significant THz signal enhancement. The data showed that maximum THz signal changed more than other pulse characteristics. Closer inspection of the data will judge how successful these particles were at improving THz pulses.

CHAPTER IV

ANALYSIS

The gathered data evaluated how gold nanoparticles modified THz pulses in a THz-TDS system. The goal of this research was to explore if gold black, colloidal gold or gold island particles applied to the surface of coplanar transmission lines would create significant signal or bandwidth increase. How well these particles improved THz pulses is analyzed in this chapter. First, the quality of each deposition is analyzed by reviewing the optical and resistance data for each chip. Next, the THz pulse data is analyzed for both focused and defocused laser beams showing how effective each deposition was at pulse enhancement. Last, possible enhancement mechanisms affecting the nanoparticles are discussed.

4.1 Gold Black Deposition

Microscope images of the gold black chips revealed gold black's characteristic dark color which steadily increased with deposition time. Gold black depositions are seen in Figures 14, 15 and 16. The first chip, with 100 seconds of gold black deposition, showed a light layer of gold black with larger scattered clumps visible. The second chip, with 300 seconds of gold black deposition, showed a darker layer across the lines. The third chip, with 1000 seconds of gold black deposition, was thick enough that the lines were

completely covered and barely visible. This layer took on a deep black color. This color is the same as the gold black samples described by Harris [25]. This color indicates that the individual gold particles have dimensions significantly smaller than the wavelength of visible light, similar to the gold black structure seen in Figure 5. Gold black had a very uniform deposition. THz pulse changes caused by gold black should vary relative to gold black deposition time.

4.2 Colloidal Gold Deposition

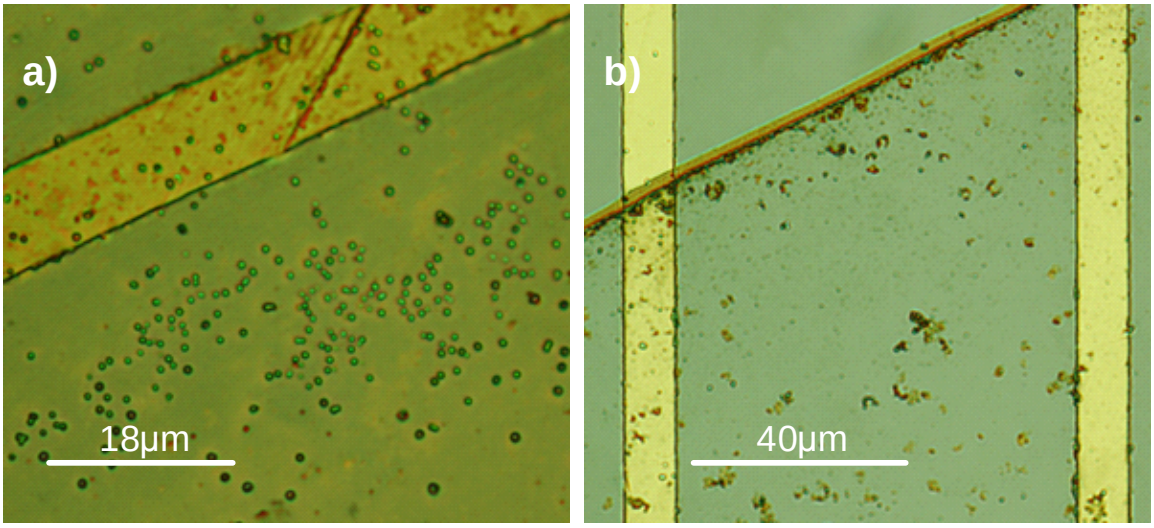

Figure 49: a) Close up of large colloidal gold nanoparticles. Gold areas of much smaller particles can be seen around the large ones. b) Image of colloidal gold particles created with different reagents. This colloidal gold solution was a red wine color, indicating different initial particle size than the particles used in this research.

Microscope images of the colloidal gold chips showed that this deposition formed unexpectedly large particles. This deposition is shown in Figures 24, 25 and 26. Large particles ≈1µm in diameter are shown in Figure 49a. These particles appeared on each chip and formed after the colloidal gold had evaporated. Preliminary SEM data was taken on a similar concentration of colloidal gold shown in Figure 7. Individual particles are

≈20nm in size. Close inspection showed much smaller particles exist on the chip, evident from lighter gold areas surrounding the larger particles, also seen in Figure 49a. To ensure that aggregation was not unique to this solution of colloidal gold, other colloidal gold solutions were allowed to evaporate on GaAs chips. These solutions were prepared at different times and with different reagents. Each colloidal gold solution formed aggregates after evaporation. It was unexpected that large particles would form from colloidal gold deposition.

Two different colors of particle were observed in this deposition. The coloration was darker on the aggregates in the undiluted solution, more closely resembling gold black deposits. The two diluted solutions had aggregates the same gold color as bulk gold. It is not clear why these aggregates formed, but it is theorized that the evaporation process upset the electrostatic forces keeping the particles separated. The dark color seen on these aggregates means they must be fairly well separated. Salts, which were more concentrated in the undiluted solution, might have kept the gold particles from making electrical contact when they aggregated. This is less likely to happen in the diluted solutions and would explain the differences in color.

Overall, colloidal gold deposition was problematic due to evaporative transport of the gold particles. Each of these chips had dense particle accumulation along the edge of the 1µL drop. The first chip, diluted to $1/16^{th}$ concentration, had a band of gold at the drop edge and much less over the center. The second chip, diluted to $1/4^{th}$ concentration, again had accumulation at the drop edge but also had large particle deposits randomly located

around the drop. The undiluted drop had more particle accumulation than the other two chips at the drop edge. It was covered more evenly in the center with dense darker colored particle groups than the previous two chips. This accumulation around the edge of the drop can be seen in Figure 26c. Particles clustered at these edges increased current flow and made it difficult to bias at greater than 21V. This limited strength of the THz pulses these colloidal gold chips could create.

Another problem with the colloidal gold deposition was that particles deposited themselves differently between chips. The coverage on the $1/4^{th}$ concentration chip was the least uniform across the transmission lines. Also the undiluted chip had different spacing and particle color than the other two chips. This made it impossible to correlate variation seen in the THz data to increasing colloidal gold concentrations. The variation inherent in colloidal gold deposition needs to be better controlled to more accurately gain meaningful THz data.

4.3 Gold Island Deposition

Microscope images show an even deposition of gold islands on the chips and coloration indicative of their structure. This deposition is seen in Figures 37, 38 and 39. Reflectivity measurements on these particles can be seen in Table 16. Reflectivity data was measured with GaAs surfaces deposited in same manner as the gold island chips. The 1nm gold island deposition was optically invisible. Reference data recorded on Table 16 showed that a 1nm gold island layer was slightly absorptive at 808nm light. The 3nm gold island chip showed up as a thin gold colored band across the sample line. This band was visible

due to the increased reflectivity of these larger island particles. The 5nm line also showed up as a band across the sample line, though for reasons not explored appeared darker on the lines themselves. After the 5nm deposition, white areas on the chip holder appeared light blue. This color is characteristic of gold island particles [45]. The chips showed even coverage across the lines and reflectivity data indicated progressive island enlargement between gold island layers. The excellent quality of gold island deposition gives additional weight to the resulting THz data.

4.4 Resistance Data

Particle deposition was also inspected electrically. Measuring the resistances across transmission lines can give additional insight into how the nanoparticles were deposited. Table 17 gives a list of approximate dark chip resistances. These approximate values were gathered from the resistance plots taken on each of the nine nanoparticle chips listed in Chapter 3. A close look at the reference lines and each deposition is given below.

Type	Amount	Reference	Sample
Gold Black	100s	350MΩ	100MΩ
	300s	100MΩ	200MΩ
	1000s	25MΩ	1MΩ
Colloidal Gold	1/16th Sol., 1μL drop	1500MΩ	4MΩ
	1/4th Sol., 1μL drop	300MΩ	7MΩ
	1μL drop	300MΩ	1MΩ
Gold Island	1nm	750MΩ	25MΩ
	3nm	750MΩ	13MΩ
	5nm	250MΩ	2MΩ

Table 17: Table of approximate resistances, taken from the darkened chip resistance plots in Chapter 3.

A base line resistance for a “blank” line can be acquired from the reference data. Table 17 shows the most common reference resistance to be ≈300MΩ. This is seen in the 5nm gold island chip, two of colloidal gold chips and the 100 second gold black chip.

Variations from this value are easily explained. The 1500 MΩ value for the 1/16 concentration colloidal gold chip is far too high indicating that something interfered with the measurement. The 750MΩ values for the 1nm and 3nm gold island chips were expected to higher than average because they were truncated lines (≈5mm long). The 100MΩ and 25 MΩ values on the gold black chips meant that slight annealing of the gold black occurred. This is discussed more in following paragraph. Overall, analysis of the reference line resistances concludes that ≈300MΩ is the base resistance across these lines.

Gold black resistance data showed that this deposition had little electrical impact on the THz transmission lines and that slight annealing occurred. The chips with 100 and 300 seconds of gold black deposition had resistances of 100MΩ and 200MΩ, respectively. This is much closer to the 300MΩ reference line resistance than the other nanoparticle depositions. This means gold black made little contact with the substrate even though it appeared visually dense on the surface. The deposition with 1000 seconds of gold black was an exception to this. The low resistance values on both the reference and sample lines indicate that slight annealing of the gold black occurred. This happened because the gas required for gold black deposition can heat up during long deposition times. This would make it possible for small amounts of gold black to melt to the surface of both reference and sample lines. This melted layer would remain on the reference line even after the rest of the gold black was removed. It is also interesting that the reference line resistance was the same as the sample line on the 1nm gold island chip. It seems that the small amount of melted gold black formed a layer electrically similar and optically

similar (invisible) to the 1nm of gold islands. The low 1MΩ sample line resistance is due to a thick layer of gold black sitting on this melted layer. The THz data will show how these different gold black depositions affected the THz pulse.

The colloidal gold resistance data gives little information about the quality of the colloidal gold deposition. Resistance data was recorded for the transmission lines as a whole. But the electrical properties of this deposition were dominated by the clusters of large aggregates located around each chip. If these clusters were rearranged the electrical properties of these lines would change. The resistance plots for these chips in Chapter 3 showed that ≈20V bias kept the current below 4mA for the chip with a $1/16^{th}$ concentration and the chip with an undiluted concentration. The particles clustered at the edges of the drops are responsible for this high current draw. This is a limitation in standard THz-TDS systems, but was worked around in this research by taking THz data at low (<20V) voltages. Electrical data would better reflect the structure of the colloidal gold nanoparticles if the particles were deposited more uniformly across the transmission lines.

The resistance data showed that the gold island deposition was the most successful nanoparticle deposition performed. Low resistance values showed that this nanoparticle made excellent electrical contact with the chip. This is attributed to the evaporative process used to deposit the gold. The resistance data also showed a steady decrease as the gold island layer became thicker. This would be expected as additional gold particles made the island layer more conductive. This deposition appeared to have less

uncontrolled variables than the gold black and colloidal gold particles. The quality of this deposition gives extra weight the gold island data collected. It is expected that this deposition will give the most reliable THz data.

4.5 Gold Black THz Data

Analysis of the THz pulses created from the gold black chips did not show significant changes in the THz pulse. This is surprising, as a drastic difference between the sample and reference lines was observed visually. The changes that were seen were changes in the maximum signal. Frequency characteristics were fairly stationary. The best improvement came from the chip with 300 seconds of gold black deposition when it was illuminated with a defocused beam. These chips showed that gold black does not provide signal enhancement useful for standard THz-TDS systems. Close examination of each chip is given below.

The first gold black chip was deposited with 100 seconds of gold black. It was basically identical to the reference pulse. The sample pulse was 25% less than the reference, but had oscillations in the frequency spectrum indicative of slight misalignment. Better alignment would boost the strength of the sample closer to that of the reference. This gold black deposition of had little effect on the resulting pulse. This chip serves as the lower bound for gold black deposition times.

The second chip had 300 seconds of gold black deposited on it. It showed the only gold black induced signal increase. This chip was scanned twice, once with a focused beam

and once with a defocused beam. It was the only gold black chip scanned with a defocused beam. The pulse created with a focused beam was close enough to the reference line to be identical. In this respect, the 100 and 300 second chips are the similar. The defocused laser beam showed a large signal increase of 52.4% over the reference. The reasons for this enhancement are unclear. It appears that some nanoparticle enhancement effect increases with larger area of illumination. Overall, however, this gold black deposition did not provide signal enhancement useful for a standard THz-TDS system because no enhancement occurred with a focused laser beam. But the signal increase using a defocused beam is interesting and could be explored in future gold black research.

The last gold black chip showed no signal improvement. This chip had 1000 seconds of gold black deposition and, like the first gold black chip, was only illuminated with a focused laser beam. The black color of this layer indicted optical absorption and the resistance data indicated it had increased electrical contact with the substrate, but neither improved the resulting THz signal. The signal was reduced by 27.6% that of the reference signal. No absorbed light seems to have injected carriers to the chip. Considering the amount of gold black on the chip, it is interesting that the signal was not reduced further. This chip showed that a very large layer of gold black does reduce the incident laser light. Further deposition of gold black would only decrease the amount of light reaching the THz emitter. Overall, gold black deposition was not successful in creating THz signal enhancement.

4.6 Colloidal Gold THz Data

Colloidal gold particles did not provide good THz signal enhancement. Pulses created from these chips showed more variation in frequency than the other depositions, but this variation was always shifted to lower frequencies. This frequency shift was not seen in other depositions and so could be due to the structure of the colloidal gold deposition. The only THz signal enhancement came from the $1/16^{th}$ diluted solution illuminated with a defocused beam. It is not known what mechanisms caused this enhancement. Observed signal loss was likely caused by thermal absorption or reflection of the incident laser light. A close examination of each chip is given below.

The first colloidal gold chip was deposited with a 1µL drop of colloidal gold diluted to $1/16^{th}$ the original concentration. This chip was scanned with a focused beam and a defocused beam. Like most of these chips, it showed signal enhancement when a defocused beam was used. The focused beam dropped the signal to 64% that of the reference and doubled the current across the sample line. The defocused beam increased signal by 41% over the reference. The current, unexpectedly, remained about the same as when a focused beam was used. Current was observed to increase with beam size. This small change in current is evidence that most of the current was coming through the gold clusters at the edge of the drop. Again, the reasons for the signal enhancement and loss are not apparent. But the large reduction in signal with a focused beam rules out this deposition for use in standard THz-TDS systems.

The second colloidal gold chip was deposited with a 1µL drop of colloidal gold diluted to $1/4^{th}$ the original concentration. Like the previous chip, it only showed signal improvement when illuminated with a defocused beam. A focused beam caused the sample pulse to reduce to 53.5% of the reference pulse, while the sample line current increased to three times that of the reference current. The THz pulse showed a strong low frequency shift and even a strange shift in the time domain pulse. This was probably due to misalignment since it disappeared when the beam was defocused. The defocused beam created a pulse with higher maximum signal than the reference pulse. The sample pulse had to be scanned at a lower bias voltage because of high current draw. But it can be seen that an additional 10V on the sample line would increase the max signal beyond the reference. It would also keep increasing current, seen in Figure 32e. It is difficult to say what could be causing this increase in signal. The signal to voltage plot from the focused chip, Figure 32.d, shows that higher voltage improves the colloidal gold signal more than the reference signal. These particles seem give an enhancement which scales with voltage. This improved voltage scaling is seen on other THz chips and discussed later in the section on enhancement mechanisms. This effect is interesting, but overall this chip did not provide useful signal enhancement because of the large signal drop seen when a focused beam was used.

The last colloidal gold chip was deposited with a 1µL drop of undiluted colloidal gold solution. It behaved similar to the previous two colloidal gold chips. It was scanned twice, once with a focused beam and once with defocused beam. The focused beam produced a signal loss that was 36% that of the reference. The defocused beam produced

a signal increase that was 18.6% over the reference. Other pulse characteristics were about the same. Current was high on this chip limiting both scans to a 20.43V bias. The current on the reference line remained the same but on the sample line increased by 2mA between the focused and defocused scans. Overall this chip only showed a small enhancement with a defocused beam and no enhancement that would be useful in a standard THz-TDS system. Further colloidal gold deposition would not improve the resulting THz pulse and would cause additional unwanted current flow.

4.7 Gold Island THz Data

Analysis of the THz pulses created from gold islands chips were more promising than either the gold black or colloidal gold chips. They showed significant increase in signal when reflectively was accounted for. The expected signal loss due to reflectivity was absent in most cases. This property helped the 3nm gold island chip better resist the effects of high laser powers. Also the only signal increase with a focused beam was observed from a 1nm gold island layer. This increase was 47.8% over the reference pulse. This enhancement is not large, but could be useful in THz-TDS systems where signal strength is paramount. A close examination of each chip is given below.

The first gold island chip showed a large frequency gain but evidence indicates this is not due to the nanoparticles. This chip was deposited with a 1nm layer of gold islands. The center frequency was shifted up 0.1209THz and the FWHM increased by 65%. It is unclear what caused this large gain in frequency. However, a similar increase in bandwidth appeared in the reference line of the defocused 3nm gold island chip. This

reference line was the same reference line used for the 1nm gold island layer. If this frequency improvement can occur on the reference line in a difference scan then it is evidently not caused by the gold island particles.

But the 1nm gold island chip did show the only THz pulse increase when using a focused laser beam. This signal had a 47.8% increase over the reference pulse. The sample line current was roughly double the reference line current. Reflectivity data showed the 1nm gold island layer to slightly absorb IR light (808nm). This signal gain cannot be accounted for by this small absorption. The signal/voltage plot in Figure 41d shows that the sample line increased with voltage at a larger rate than the reference line. The chip was biased at 45V when the THz pulse was recorded. This voltage was well into the region where the sample pulse gained more from voltage than the reference. It is unclear what is causing this enhancement but it appears that voltage positively affects it. Because this enhancement was observed with a focused beam, it can be used in a standard THz-TDS system. Also gaining more THz signal relative to voltage is desirable, as long as current does not become too high. Overall the 1nm gold island layer had the most useful results seen in this research.

The second gold island chip showed signal loss with a focused beam and slight enhancement with a defocused beam. This chip was deposited with a 3nm layer of gold island particles. Differences between beam sizes were unexpected because of the small size of gold islands relative to the sizes of the focused and defocused beams. The focused beam had about the same signal level as the reference pulse and was shifted toward lower

frequencies. This could have been due to misalignment because this frequency shift disappeared when the defocused beam was used. When using a defocused beam, the maximum signal increased to 25.3% over the reference. This is a small increase and drew a low level of current, the same as the reference line. But this signal enhancement is interesting because 3nm gold islands reflect 16% of the incident light. Preliminary data indicated this corresponds to roughly a 30% decrease in THz signal. Together this is equivalent to an increase of 63% over the reference. This is a large improvement over previously observed pulses. Overall no signal enhancement was seen with a focused beam so this deposition would not be useful for a standard THz-TDS system, but the ability of this chip to maintain signal despite reflectivity losses was worth further exploration. Data from this chip was taken with a high powered defocused beam and displayed in Figure 48.

The third gold island chip had a 5nm layer of gold islands deposited on it. These particles are larger than the 1nm and 3nm gold island particles and the distance between them is smaller. The THz pulse created with a defocused beam had a large and significant drop in signal. It dropped 53.9% that of the reference signal. Reflectivity data showed that 5nm islands reflected 36% of incoming light. Preliminary data showed this roughly corresponded to a 60% drop in THz signal. Interestingly, this was close to the amount of signal drop observed. This means the enhancement effects that overcame reflectivity losses on the previous chip did not seem to be effective on the 5nm gold island chip. However, the THz pulse created with a focused laser beam had the opposite effect. This created a pulse almost identical to the reference pulse. Accounting for reflectivity loss

this became an increase of 51.3% over the reference pulse. The cause of this dramatic attenuation and enhancement was not clear. This was the most dynamic signal change observed in this research and showed that these particles do have an effect on THz chips. Overall this deposition was interesting, but not useful. The nanoparticle effects caused by 5nm gold islands are drastic enough to merit future study, but did not produce the signal enhancement sought for in this research. Any thicker layer of gold island particles would only further reflect laser light.

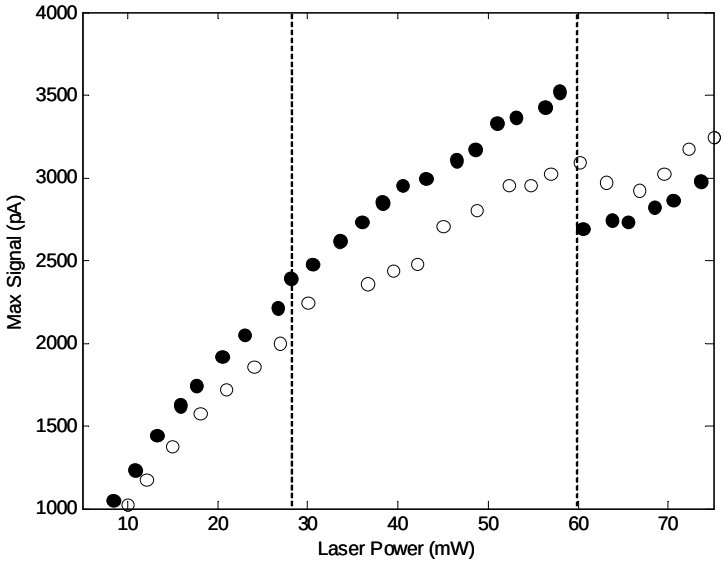

Figure 50: High power data taken from Figure 48. The bold data points are the sample line. Its laser power has been scaled by 16% to account for the light loss due to reflectivity. This was measured on the 3nm of gold islands with a defocused laser beam. The vertical dashed lines show where signal stability changes.

The goal of the research is to create stronger THz signals. One way to do this would be by creating a chip more resilient to laser light. High laser power data was recorded for the 3nm gold island chip with a defocused beam. This layer of gold islands kept a high signal while reflecting 16% of the light. Figure 48 shows the recorded high laser power data. The sample and reference line are about the same until 30mW. From 30mW to 50mW both maximum signal measurements start to become unstable, but more so for the

reference line. At 50mW to 70mW they both become unstable. The gold island line seems to retain stability for longer. Figure 50 shows this same plot shifted to account for the 16% reflected laser power. Now the plot shows the actual laser power the chip was receiving on the sample line. Similarities are immediately noticeable. At 28V there starts to be a change in stability for both lines and at 60V both lines see a signal drop. This plot shows that a chip covered in 3nm gold island particles can take 16% more laser light while maintaining signal stability.

4.8 Enhancement mechanisms

Metal nanoparticles can create enhanced electric fields in a number of ways. Papers describing these enhancement mechanisms were described in Chapter 1. Work by Osawa showed that an IR beam created a strong electric field between elliptical metal nanoparticles placed on non-reflective surfaces [46]. Principles from that work were used to explain the THz signal improvement observed with nanopores [21] [22]. Work by Cai showed that sharp transmission line features created areas of high voltage which gave THz signal enhancement [19]. Work by Fedorovich showed that areas of high voltage formed across metal island films. The voltage is high enough in these areas to emit electrons and photons [21]. This research aimed to build on the work performed by Cai through using the nanoparticle effects documented by Fedorovich. These effects are enhancement mechanisms that could improve THz pulses. Various enhancement mechanisms were considered when taking data, but no additional data was taken to explore them. Exploring specific nanoparticle enhancement mechanisms was beyond the scope of this research. But by analyzing the data and reviewing pervious work a

hypothesis can be formed about the attenuation and enhancement mechanisms affecting these particles.

Some amount of signal loss is always caused by these gold nanoparticles. A conductive layer on the surface of a THz emitter can be detrimental to a THz emitter in two ways. The first comes from the nanoparticles being too conductive. This starts to affect the emitter in the same way a solid conductive sheet would. The lowered resistance draws excessive amounts of current. Increased current lowers bias voltages, can decrease the lifetime of a THz emitter and could possibly destroy transmission lines. Increased current was observed across most of these chips with colloidal gold chips drawing the most. The second method comes from blocking incident laser light. Placing particles on the surface of a chip will always interfere with some fraction of the incident light. This reduces photon energy delivered to the semiconductor substrate. Light is blocked by either being reflected or by being thermally absorbed. Any observed enhancement from these nanoparticles had to overcome these two detrimental effects.

Signal enhancement appears to come from regions of high voltage throughout the nanoparticle layers. The enhancement mechanisms described by Fedorovich are the most plausible [21]. They describe voltage induced “hot spots” in the metal island layer and similar effects induced by high laser powers. Data from the THz signal and voltage plots showed that signal strength scaled with voltage, more so than the reference signal. It is hypothesized that charge percolates through the nanoparticle layer creating regions of high field which emit photons and electrons into the substrate. These “hot spots” would

respond to increased voltages in the same way as voltage singularities caused by sharp features [19]. Fedorovich also showed that an IR beam can cause emittion of photons and electrons. The intensity required to do so was $10^4 W/cm^2$. The intensity of the focused and defocused beams used in this research were 10^{10} W/cm^2 and 10^7 W/cm^2, respectively. Both sizes of beams were intense enough to cause emission from these nanoparticles. This might explain why the THz signal also seemed to improve when a defocused beam was used. Electrons emitted from the gold due to high voltage regions and the laser beam would positively affect the THz pulse if absorbed by the GaAs substrate. This hypothesis seems to be supported by the data.

4.9 Conclusion

The recorded THz data was carefully reviewed. How the particles were deposited was important because it determined their structure and, in turn, how they affected the THz pulses. Gold black was shown to make little contact with the substrate and to anneal during long deposition times. Colloidal gold aggregated during evaporation and collected problematically around the chip. Gold island particles had a high quality deposition. Each of these particles caused an increase in the THz signal, but never more than 52.4% of the reference pulse. This increase was smaller than desired and, in all but one case, created with a defocused laser beam. A defocused beam is not used in standard THz-TDS systems. Gold Islands had the most repeatable deposition and showed the only signal increase with a focused beam. When the reflectivity of these particles is accounted for, the signal increase is larger. This is strong evidence that some form of enhancement is occurring on the gold island chips. Gold black and colloidal gold particles would not be

useful in THz-TDS applications, but gold island particles could be. Future research will need to be performed to validate the exploratory analysis performed in this work.

The goal of this research was to discover if gold nanoparticles could create a cost effective way to improve THz emitters in THz-TDS systems. This analysis showed that large signal improvements were not observed when these nanoparticles were deposited on GaAs chips. This discovery fulfilled the purpose of this research. In future work, other nanoparticles can be tried, but few will have the high conductivity, oxide resistance, ease of creation, and available nanostructures that characterized the nanoparticles used in this work. Also more elaborate deposition methods could be performed, but that would increase the cost associated with using these nanoparticles. Additional avenues of study are available from this work, including a thorough study of gold island particles. Additional work can also be performed on nanoparticle enhancement mechanisms. This chapter concludes the research performed on enhancing THz pulses through gold black, colloidal gold and gold island deposition.

CHAPTER V

CONCLUSIONS AND FUTURE WORK

THz pulses created from THz emitters coated in gold nanoparticles were created and analyzed. It was concluded that gold nanoparticles did not create significant increase in bandwidth and signal for THz emitters. This chapter summarizes the conclusions and accomplishments of this research. It also proposes possible avenues of future work. Specifically, this chapter discusses the challenges overcome, experimental accomplishments, key discoveries, future deposition improvements and future THz applications.

5.1 Challenges

This project had to overcome numerous challenges. One of the most difficult aspects of this work was dealing with the precise nature of these measurements. THz pulses were subject to many random variables including thermal instability in the laser beam and constant realignment of the optics. This is one reason why only large increases in THz signal were considered significant. This challenge was overcome by taking the time to make sure each THz pulse was properly maximized. Another challenge in this research was creating and depositing the gold nanoparticles. Gold black required special modification of the Edwards Auto 306 thermal evaporator to account for the atmosphere

during deposition. This unexpectedly introduced contamination from the tungsten filament. Numerous attempts to correct this were tried until it was discovered that burning out the oxygen before deposition would effectively remove the contamination. Colloidal gold deposition faced similar challenges. Various deposition methods were attempted and contamination from salts in the solution had to be removed. Evaporating a drop of colloidal gold at room temperature turned out to be the best method, but this could still be improved upon. Salt removal was discovered to be effectively performed with DI water. Cleaning and masking reference lines for each deposition was also challenging. The thin gold transmission lines could easily be peeled off the GaAs chip. For excessively dirty chips only direct application of acetone with a Q-tip would adequately clean them. Time was saved by ensuring that chips never became dirty in the first place. Constant attention was required during cleaning and afterward each transmission line had to be thoroughly inspected under a microscope. These same challenges will be faced in future chip depositions.

5.2 Experimental accomplishments

This work was important because it built equipment useful for THz work at OSU. During the course of this research a new THz emitting unit, linear stage and gold black adapter were constructed. The THz emitting unit was described in Chapter 2 and shown in Figure 9. It consisted of the GaAs chip, lenses, stages, and a magnetic base. It was capable of rapid chip replacement. Prepared chips were mounted on Macor disks and could be replaced in minutes with minimal impact on system alignment. Without this unit replacing chips would have been too time-consuming. The linear stage, also described in

Chapter 2, was a significant cost savings over other stages used at OSU. This stage saved thousands of dollars and served as a template for future less cumbersome THz systems. It also allowed the entire THz experiment, minus the laser, to be portable. The adapter used for gold black deposition was designed to allow deposition in the Edwards Auto 306 thermal evaporator. Gold black must be deposited close to the filament because of the small mean free path of gold atoms in a nitrogen atmosphere. This device also served as a heat sink for the GaAs chips and was equipped with an aluminum shield to avoided tungsten trioxide contamination. Gold black could not have been successfully deposited without it. This device easily attaches to the evaporator and is controlled with the shutter level. Future depositions of gold black will need this adaptor. These three devices were used to complete this research and are now part of the THz tool set used at OSU.

5.3 Key Findings

This research made some key discoveries useful to THz science. The goal of this work was to see if gold nanoparticles, which are relatively inexpensive to deposit, would significantly enhance THz pulses. A significantly enhanced pulse would have a high frequency shift, larger FWHM, or doubled maximum THz signal. This research showed that none of these criteria were met through gold nanoparticle deposition. This research showed that frequency changes were minimal, if not negative, and signal enhancement was never more than 52.4% more than the reference. This result means that the large signal improvements observed from better THz chip substrates and transmission line designs cannot be achieved by surface depositing of these nanoparticles. This result is useful because it shows that other avenues of innovation must be explored to achieve

large gains in THz signals. But the findings from this research do have future application. Gold Island particles could potentially give THz emitters an increase in signal. Depositing a 1nm layer of gold island particles on a THz emitter gave a signal increase of 47.8% more than the reference. It worked with a focused laser beam, scaled with voltage and could be easily deposited. However, more work will need to be done to validate this enhancement. Better understanding of this enhancement will lead to better application of gold island layers on future THz emitters. This research also showed signal improvement when using a defocused beam with nanoparticles. A 3nm layer of gold islands was shown to potentially protect a chip from high powered laser light while keeping the same signal strength. Traditional THz-TDS systems only use focused laser beams, but this finding could be useful in large aperture THz emitters [47] that use large high powered beams. This and the other findings from this research are useful to THz science.

5.4 Improvements

After reviewing this research, several ways to improve the quality of the nanoparticle depositions were observed. Possible improvements could be made in how gold black is deposited, how colloidal gold is deposited and how GaAs oxide growth is handled. These changes would improve the magnitude and reliability of the data collected from these nanoparticles.

Gold black deposition could be improved by creating better gold black reference lines and cooling the chips during long deposition times. The resistance data showed that gold

black reference lines were not entirely free of gold black after being cleaned. A solution to this would be to mask the lines before each deposition. This would ensure that no gold black collected on the reference lines in the first place. Masking the reference lines must be performed carefully since many substances will melt during gold black deposition. Keeping the gold black chips cool was shown to be more challenging than thought. Resistance data showed that some annealing occurred. A liquid cooling device could be built to remove excess heat from the chip holder, but that might be time and cost prohibitive. Another possible solution would be to use a larger chip holder to make a better heat sink and to refrigerate it before each use. This would be easy to make and might solve the heating problem. These improvements would create more reliable gold black THz data.

Improvements could be made to colloidal gold deposition. The large current draw caused by clusters of particles at the edge of each evaporated drop was problematic. This limited the voltages these lines could be biased by. Current draw could be reduced by removed the particles at the edges of each drop. This could be done mechanically with a fine probe or by masking all but the center of each drop. Colloidal gold deposition would also benefit from better control over the sizes of particles formed. Many of the particles formed from evaporation were much larger than desired. Turkevich added 0.01% of gelatin to his samples to prevent colloidal gold particles from aggregating [48]. This could be employed to reduce the size of colloidal gold particles and then could then be chemically removed. This would improve colloidal gold deposition and help it create better THz data.

One potentially problematic element in all these depositions was the formation of GaAs oxide. GaAs oxide electrically insulates the GaAs chip from the chip's surface. This could possibly interfere with enhancement caused by these particles. During THz chip fabrication this layer is rarely handled because it grows slowly and is only a few nanometers thick. Because this research took months to complete it could have allowed an oxide layer to grow. Oxide can be better handled by etching it away before each nanoparticle deposition. Then each chip should be immediately scanned. For long term storage, a dielectric layer transparent to IR could be placed on the gold island and colloidal gold chips to seal out oxygen from the air. Any such layer would destroy gold black particles. This would ensure THz data is not affected by this layer.

5.5 Future Work

The results of these experiments uncovered two possible forms of THz enhancement outside the scope of this work. The first uses colloidal gold particles to create voltage singularities between the transmission lines using lithographically placed masks. The second uses gold black and gold island particles to enhance large aperture THz emitters. These techniques are described below, but research showing their effectiveness is left for future work.

Using colloidal gold to create voltage singularities is an extension of the work done by Cal [19] described in Chapter 2. The work done by Cal was limited by the minimum feature size allowed through lithography. Colloidal gold particles are very small. When a

drop of colloidal gold is allowed to evaporate it will form fractal networks only a few particles wide. Fractal networks create smaller features than sharp metal features created though lithography, which also create stronger voltage singularities. Colloidal gold particles, unlike the deposition performed in this research, can be shaped into a sharp point by using a mask on the transmission lines. A mask would cover all but a triangular region on the anode. After colloidal gold deposition, the mask would be removed shaping the colloidal gold into a point, as illustrated in Figure 53. This would concentrate the electric field across these particles to a single point and lessen the influence of neighboring particles at that point. THz pulses made from shaped nanoparticle features have the potential to create stronger THz pulses than those create from sharp metal features.

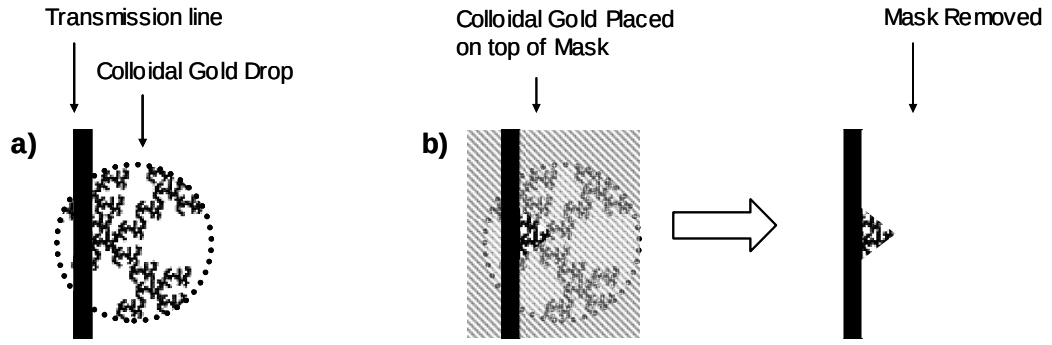

Figure 53: a) Shows a colloidal gold drop placed over the anode of a THz transmission line. b) Shows a colloidal gold drop placed on a line that has been masked. When the mask is removed sharp features are created from the remaining colloidal gold.

Large aperture THz emitters can be enhanced by the nanoparticles studied in this research because these emitters use large beam sizes. Large aperture THz emitters have transmission lines separated by several millimeters and are biased by several kilovolts [47]. Beam sizes are several millimeters in diameter. The high voltages used in large aperture THz experiments make them more dangerous to perform, but they produce much

more powerful THz pulses than traditional THz emitters. This research showed better signal improvement when nanoparticles were illuminated with larger beam sizes. This effect works perfectly with the design of large aperture emitters. The beam in these emitters is hundreds of times larger than the defocused beam used in this research. Larger beam sizes would allow much greater interaction between the beam and the nanoparticles creating a much stronger affect on the resulting THz pulse. How well these gold nanoparticles could improve large aperture emitters will need to be explored experimentally. But this research indicates gold nanoparticles would have a positive effect on large aperture THz emitters.

5.6 Conclusion

This research explored THz enhancement using cost effective techniques and materials. The key discoveries made from this research were that surface deposition of gold nanoparticles did not create large THz signal enhancement, but that gold island particles could potentially provide useful smaller signal enhancement. OSU labs gained equipment specific deposition techniques as well as the hardware created to perform this research. This work naturally applies to large aperture THz emitters due to the almost universal signal improvement seen when using a defocused laser beam. Overall this research explored an interesting and interdisciplinary avenue of THz science and successfully fulfilled the requirements of a master's degree.

REFERENCES

1. Vanexter, M. and D.R. Grischkowsky, *characterization of an optoelectronic terahertz beam system.* Ieee Transactions on Microwave Theory and Techniques, 1990. **38**(11): p. 1684-1691.
2. Fattinger, C. and D. Grischkowsky, *point-source terahertz optics.* Applied Physics Letters, 1988. **53**(16): p. 1480-1482.
3. *TeraView terahertz technology for 3D imaging and spectroscopy*. March 09, 2009; Available from: http://www.teraview.com/terahertz/.
4. *Merlijn Hajenius obtains PhD on nano-detector for remote cosmic realms*. 2007; Available from: http://www.tnw.tudelft.nl/live/pagina.jsp?id=e93926d3-0cf0-4456-bdc9-931fc1dde5e2&lang=en.
5. *New T-ray Source Could Improve Airport Security, Cancer Detection*. 2007; Going through airport security can be such a hassle. Shoes, laptops, toothpastes, watches and belts all get taken off, taken out, scanned, examined, handled and repacked. But "T-rays", a completely safe form of electromagnetic radiation, may reshape not only airport screening procedures but also medical imaging practices.]. Available from: http://www.newswise.com/p/articles/view/535615/.
6. *Checking people at airports - with terahertz radiation*. 2008; Available from: http://www.ptb.de/en/aktuelles/archiv/presseinfos/pi2008/pitext/pi080918.html.
7. W.J. Gallagher, C.-C.C., I.N. Duling III, D. Grischkowsky, N.J. Halas, M.B. Ketchen, and A.W. Kleinsasser, *Subpicosecond Optoelectronic Study of Resistive and Superconductive Transmission Lines.* Applied Physics Letters, 1987. **50**.
8. McGoverin, C.M., T. Rades, and K.C. Gordon, *Recent Pharmaceutical Applications of Raman and Terahertz Spectroscopies.* Journal of Pharmaceutical Sciences, 2008. **97**(11): p. 4598-4621.
9. Zhong, H., et al., *Nondestructive defect identification with terahertz time-of-flight tomography.* Ieee Sensors Journal, 2005. **5**(2): p. 203-208.
10. Kawase, K., et al., *Non-destructive terahertz imaging of illicit drugs using spectral fingerprints.* Optics Express, 2003. **11**(20): p. 2549-2554.
11. Schmuttenmaer, C.A., *Exploring dynamics in the far-infrared with terahertz spectroscopy.* Chemical Reviews, 2004. **104**(4): p. 1759-1779.
12. Trager(Ed.), F., *Springer Handbook of Lasers and Optics*. 2007, LLC New York: Springer Science+Business Media.
13. Ralph, S.E. and D. Grischkowsky, *trap-enhanced electric-fields in semi-insulators - the role of electrical and optical carrier injection.* Applied Physics Letters, 1991. **59**(16): p. 1972-1974.
14. Vanexter, M., C. Fattinger, and D. Grischkowsky, *high-brightness terahertz beams characterized with an ultrafast detector.* Applied Physics Letters, 1989. **55**(4): p. 337-339.

15. Vanexter, M. and D. Grischkowsky, *carrier dynamics of electrons and holes in moderately doped silicon.* Physical Review B, 1990. **41**(17): p. 12140-12149.
16. Katzenellenbogen, N. and D. Grischkowsky, *efficient generation of 380 fs pulses of thz radiation by ultrafast laser-pulse excitation of a biased metal-semiconductor interface.* Applied Physics Letters, 1991. **58**(3): p. 222-224.
17. Gupta, S., et al., *subpicosecond carrier lifetime in gaas grown by molecular-beam epitaxy at low-temperatures.* Applied Physics Letters, 1991. **59**(25): p. 3276-3278.
18. Brener, I., et al., *Terahertz emission from electric field singularities in biased semiconductors.* Optics Letters, 1996. **21**(23): p. 1924-1926.
19. Cai, Y., et al., *Design and performance of singular electric field terahertz photoconducting antennas.* Applied Physics Letters, 1997. **71**(15): p. 2076-2078.
20. Melloch, M.R., et al., *low-temperature-grown iii-v materials.* Annual Review of Materials Science, 1995. **25**: p. 547-600.
21. Fedorovich, R.D., A.G. Naumovets, and P.M. Tomchuk, *Electron and light emission from island metal films and generation of hot electrons in nanoparticles.* Physics Reports-Review Section of Physics Letters, 2000. **328**(2-3): p. 74-179.
22. Wilkinson, P.G. and L.S. Birks, *particle size of evaporated gold.* Journal of Applied Physics, 1950. **21**(1): p. 60-60.
23. Harris, L., R.T. McGinnies, and B.M. Siegel, *the preparation and optical properties of gold blacks.* Journal of the Optical Society of America, 1948. **38**(7): p. 582-589.
24. Advena, D.J., V.T. Bly, and J.T. Cox, *deposition and characterization of far-infrared absorbing gold black FILMS.* Applied Optics, 1993. **32**(7): p. 1136-1144.
25. Harris, L. and J.K. Beasley, *the infrared properties of gold smoke deposits.* Journal of the Optical Society of America, 1952. **42**(2): p. 134-140.
26. Forrest, S.R. and T.A. Witten, *long-range correlations in smoke-particle aggregates.* Journal of Physics a-Mathematical and General, 1979. **12**(5): p. L109-L117.
27. Sotelo, J.A., V.N. Pustovit, and G.A. Niklasson, *Optical constants of gold blacks: Fractal network models and experimental data.* Physical Review B, 2002. **65**(24).
28. Oneill, P., C. Doland, and A. Ignatiev, *structural composition and optical-properties of solar blacks - gold black.* Applied Optics, 1977. **16**(11): p. 2822-2826.
29. Niklasson, G.A. and C.G. Granqvist, *infrared-optical properties of gas-evaporated gold blacks - evidence for anomalous conduction on fractal structures.* Physical Review Letters, 1986. **56**(3): p. 256-258.
30. Niklasson, G.A., *optical-properties of gas-evaporated metal particles - effects of a fractal structure.* Journal of Applied Physics, 1987. **62**(1): p. 258-265.
31. Turkevich, J., P.C. Stevenson, and J. Hillier, *a study of the nucleation and growth processes in the synthesis of colloidal gold.* Discussions of the Faraday Society, 1951(11): p. 55-&.
32. Saraiva, S.M. and J.F. de Oliveira, *Control of particle size in the preparation of colloidal gold.* Journal of Dispersion Science and Technology, 2002. **23**(6): p. 837-844.

33. Chow, M.K. and C.F. Zukoski, *gold sol formation mechanisms - role of colloidal stability.* Journal of Colloid and Interface Science, 1994. **165**(1): p. 97-109.
34. Weitz, D.A. and M. Oliveria, *fractal structures formed by kinetic aggregation of aqueous gold colloids.* Physical Review Letters, 1984. **52**(16): p. 1433-1436.
35. Chavez, I.M., Brian; Ojha, Lawanya; Oswald, Nick; Topal, Ozge, *Lab 3, Observation of Self Assembly* in *Nanotechnology Course*. 2007, Oklahoma State University Stillwater, Oklahoma.
36. Osawa, M., *Dynamic processes in electrochemical reactions studied by surface-enhanced infrared absorption spectroscopy (SEIRAS).* Bulletin of the Chemical Society of Japan, 1997. **70**(12): p. 2861-2880.
37. Kalyuzhny, G., et al., *UV/vis spectroscopy of metalloporphyrin and metallophthalocyanine monolayers self-assembled on ultrathin gold films.* Journal of Physical Chemistry B, 2000. **104**(34): p. 8238-8244.
38. Walther, M., et al., *Terahertz conductivity of thin gold films at the metal-insulator percolation transition.* Physical Review B, 2007. **76**(12).
39. Gompf, B., et al., *Nanometer-thick Au-films as antireflection coating for infrared light.* Optics Letters, 2007. **32**(11): p. 1578-1580.
40. Tu, J.J., C.C. Homes, and M. Strongin, *Optical properties of ultrathin films: Evidence for a dielectric anomaly at the insulator-to-metal transition.* Physical Review Letters, 2003. **90**(1): p. 4.
41. Newport, *The Newport Resource*, Newport, Editor. 2009. p. 804.
42. Aperture, N., *Motion Control Catalog*, N.A. Inc., Editor. 2009. p. 19.
43. Zhang, W., *Embedded GaAs THz Chip Processing*. 2003. p. 2.
44. McKenzie, D.R., *selective nature of gold-black deposits.* Journal of the Optical Society of America, 1976. **66**(3): p. 249-253.
45. Miyake, H., S. Ye, and M. Osawa, *Electroless deposition of gold thin films on silicon for surface-enhanced infrared spectroelectrochemistry.* Electrochemistry Communications, 2002. **4**(12): p. 973-977.
46. Osawa, M. and M. Ikeda, *surface-enhanced infrared-absorption of para-nitrobenzoic acid deposited on silver island films - contributions of electromagnetic and chemical mechanisms.* Journal of Physical Chemistry, 1991. **95**(24): p. 9914-9919.
47. Hu, B.B., et al., *optically steerable photoconducting antennas.* Applied Physics Letters, 1990. **56**(10): p. 886-888.
48. Turkevich, J., G. Garton, and P.C. Stevenson, *the color of colloidal gold.* Journal of Colloid Science, 1954. **9**(6): p. S26-S35.

VITA

Christopher Dall Young

Candidate for the Degree of

Master of Science

Thesis: EXPLORING TERAHERTZ EMITTER CHANGES THROUGH NANOPARTICLE DEPOSITION

Major Field: Electrical and Computer Engineering

Biographical:

Personal Data:

Education:
Completed the requirements for the Master of Science of Electrical and Computer Engineering at Oklahoma State University, Stillwater, Oklahoma in May 2009

Completed the requirements for the Bachelor of Science of Electrical and Computer Engineering at Brigham Young University, Provo, Utah in August 2006

Name: Christopher Dall Young Date of Degree: May 2009

Institution: Oklahoma State University Location: OKC or Stillwater, Oklahoma

Title of Study: EXPLORING TERAHERTZ PULSE ENHANCEMENT THROUGH NANOPARTICLE DEPOSITION

Pages in Study: 78 Candidate for the Degree of Master of Science

Major Field: Electrical and Computer Engineering

Scope and Method of Study: This research explored the resulting terahertz pulses created from terahertz coplanar transmission lines deposited with gold black, colloidal gold and gold island nanoparticles. The small feature size of these particles caused areas of high voltage throughout the nanoparticle layer. Analysis of the resulting terahertz pulses showed whether these areas of high voltage affected the electric field across the terahertz transmission lines.

Findings and Conclusions: Gold black, colloidal gold and gold islands were deposited on separate terahertz coplanar transmission lines. The quality of each deposition was evaluated and terahertz pulses from these lines were recorded and analyzed. This work found that these nanoparticles did not significantly increase the terahertz signal or bandwidth. Gold black and colloidal gold particles created a loss in terahertz signal. However, a small signal gain was observed with a 1nm gold island layer. Also 3nm and 5nm gold island layers were observed to maintain signal strength even with laser light loss due to reflectivity. Out of the nanoparticles explored, gold island particles are worth additional of study.

ADVISER'S APPROVAL: Dr. Alan Cheville